ISSN 0736-5306

SCIENCE OF TSUNAMI HAZARDS

The International Journal of The Tsunami Society

Volume 8 Number 2 1990

OBJECTIVE: The Tsunami Society publishes this journal to increase and disseminate knowledge about tsunamis and their hazards.

DISCLAIMER: The Tsunami Society publishes this journal to disseminate information relating to tsunamis. Although these articles have been technically reviewed by peers, The Tsunami Society is not responsible for the veracity of any statement, opinion, or consequences.

Submit manuscripts of articles, notes, or letters to:

T. S. Murty Technical Editor
Institute of Ocean Sciences
Department of Fisheries and Oceans
Sidney, B.C., Canada V8L 4B2

If article is accepted for publication the author(s) must submit a camera ready manuscript. A voluntary $50.00 page charge will include 50 reprints.

SUBSCRIPTION INFORMATION: Price per copy $20.00 USA

ISSN 0736-5306

Published by **The Tsunami Society** in Honolulu, Hawaii, U.S.A.

TSUNAMI TRAVEL TIME CHARTS FOR THE CARIBBEAN[1]

Thomas P. Weissert
Department of Physics
University of Colorado
Boulder, CO 80309

ABSTRACT

We are adapting a tsunami travel-time chart program, originally designed for the Pacific Ocean region, to generate charts for tsunamis in the Caribbean—a region of historical tsunami hazard. The program employs a cycloid curve fit to determine the path of least time for a linear long wavelength gravity wave whose wave-speed is proportional to the square root of the depth. The program requires a rectangular bathymetry grid input and prints out a text file map of the region with wavefronts at specified intervals. The estimated time for a complete crossing of the Caribbean is 3.2 hrs. laterally and 1.5 hrs. meridionally. High resolution local bathymetry, at the 15 second range, is required for island-to-nearby-island estimations. The program has not been calibrated due to the lack of historical reference time data in this region. Expected improvements for the program's performance include a contour plotting routine, finer mesh bathymetry, calibration, and perhaps amplitude prediction. This program could function well as one part in a much needed hazard warning system for the area.

[1]This study was supported by CIRES at the University of Colorado and the National Geophysical Data Center of NOAA

INTRODUCTION

The Caribbean Sea area has been racked by earthquakes and their accompanying tsunamis. Whereas the hazard presented by tsunamis in the Pacific basin is well known and well documented, not much attention has been paid to its counterpart in the Caribbean. Most of the work done with computer simulation of tsunami generation and propagation has been directed toward preventing loss of life and property in the highly populated areas of the Pacific basin. We are applying some of that body of work to the Caribbean Sea region. Specifically, we have obtained a tsunami travel time calculation program, originally designed for use in the Pacific, and converted it to function in the Caribbean.

The Puerto Rico–Virgin Islands region should be considered one of considerable seismic risk. In their global assessment of seismic potential, McCann et al. (1979) include a part of this region in a special category along with the Commander Islands in the westernmost Aleutians, and the Andaman-Nicobar region in the Indian Ocean. In each of these three regions the occurrence of a large earthquake is considered likely despite the lack of evidence of a major event within the last century. These events are still plausible because the seismic potential assignment is considered poorly constrained. But for most of the Caribbean plate boundary, McCann et al. assign their highest potential for seismic activity, which they color red on their chart. The Caribbean plate is estimated to move in relation to the North and South American plates at a rate of 2 cm/yr (Jordan, 1975). Thus 2 meters of potential slip could accumulate in 100 years. Because the indicated plate motion is towards the WSW, the region near the Greater Antilles Islands would be expected to experience only strike-slip earthquakes. This is the region which is similar to the Commander Islands. And thus, since the latter region may have experienced a large interplate event in 1858 (Sykes et al. , 1981), it is reasonable to postulate the Puerto Rico-Virgin Islands region to be also one of considerable tsunamic-seismic risk (McCann, et al. , 1979). But it is the vertical motion of thrust-type earthquakes which one would expect to be tsunamigenic. Thus the expected underthrusting along the Lesser Antilles arc would seem to be a potential source of future tsunamis, although a 100 year recurrence time may be a low estimate. Given this speculation about seismic potential, let us consider the evidence of two significant events within the region.

In the last several hundred years several tsunamigenic earthquakes have occurred in the Puerto Rico-Virgin Islands region. The two largest of these were the Virgin Islands earthquake of 1867 (Reid and Taber, 1920) and the Puerto Rico earthquake of 1918 (Reid and Taber, 1919). Whereas Reid and Tabor place the epicenter of the 1867 earthquake 15 kilometers south of St. Thomas (in the Virgin islands), a comparison of the time separation between the reports of the seismic shock and the tsunami's arrival at Charlotte Amalie (about 20 minutes) indicate that the epicenter must have been further away. Strong tsunamis were reported on the islands of St. Thomas and St. Croix. At the harbor entrance of St. Thomas the wave was reported to have a height of 6 m, decreasing to 2.5 m at the shore. This tsunami was also noticeable throughout the Lesser Antilles Islands. The earthquake of 1918 occurred about 15 km off the northwest coast of Puerto Rico and generated a wave of 4.5 to 6 m, observed all along the western coast of Puerto Rico and as far away as the Dominican Republic (at about 1 m). The estimated damage in Puerto Rico due to this earthquake and the accompanying tsunami was a loss of one hundred and sixteen lives and property damage in excess of 4 million (1918) dollars.

In addition to tsunamis generated within the region, the islands are also susceptible to tsunamis generated by distant earthquakes. The great Lisbon, Portugal earthquake of 1755 produced a large tsunami which was observed all along the Lesser Antilles Islands as well as the Portuguese, Spanish, and North African coasts. The reports of this wave claim heights of 3.5 m at Antigua and Barbados, and 6 m at Saba (Mallet, 1852).

TRAVEL TIME PROGRAM

In order to bring the methods and techniques developed for tsunami prediction and warning from the Pacific basin to the Caribbean, we have obtained a computer program developed by Masami Okada of the Seismology and Volcanology Division of the Meteorological Research Institute of Japan. The program, called SEIJI, takes the coordinates of a tsunami source and propagates the wave outward, calculating travel times for each point on a specified geographical grid. The final output of the program is a travel time chart showing consecutive wavefronts emanating from the source (Figures 3 and 4). We modified this program to run on our VAX 8550, using bathymetric data for the Caribbean region.

The program assumes linear gravity wave theory and is thus only valid for deep water propagation. The fact that the linear theory breaks down in shallow water separates the propagation problem from the run-up problem. The program also assumes the long wavelength approximation, which is certainly valid for tsunamis propagating in the Caribbean. Tsunamis typically have wavelengths greater than 100 km and the Caribbean has an average depth of 4 km. This theory under these assumptions predicts a wave speed that depends only on depth.

$$v(x,y) = \sqrt{gz(x,y)} \tag{1}$$

Because we are interested in making travel time charts and since the wave speed depends on depth, we needed to supply the program with bathymetric data for the Caribbean. We obtained a section of the ETOPO5 5-minute Gridded World Elevations for the entire Caribbean region from the National Geophysical Data Center, and a partial set of 15-second gridded NOS Hydrographic data for the area surrounding Puerto Rico and the U.S. Virgin Islands. Due to the incompleteness of the NOS data, thus far we have only converted the ETOPO5 data to the program's format.

Whereas the program automatically uses the finest gridded bathymetry available to it, usually the scale of the travel time chart requires a finer mesh of points than is possible with any available bathymetry. But even more important than the scale size of the output map, is the fact that the time travel integral must be numerically integrated along a path which requires depth values spaced sufficiently close to facilitate the step size of the numerical procedure. In order to obtain depth values for all points of calculation, the program must interpolate to points lying between the supplied data mesh. SEIJI interpolates the depth at any point by first mapping the rectangular bathymetry grid into a 60–120 degree parallelogram—which can be completely subdivided into equilateral triangles (see figure 1). Since three points determine a plane, each triangle of the grid has a depth plane fitted to it using the depths at the three points which define it. Once the travel times are calculated for all required points within the parallelogram, the grid is inversely mapped back into the rectangular form and the travel time chart is generated. The interpolated depth at any point is a function of its coordinates (x,y) according to

$$z(x,y) = \alpha x + \beta y + \gamma \tag{2}$$

where α, β, and γ are determined by the three-point depth plane. Once a depth plane is fitted to a triangular region, the following coordinate transformation is performed

$$X = \frac{1}{\sqrt{\alpha^2 + \beta^2}}(\beta x - \alpha y) \tag{3}$$

$$Y = \frac{1}{\sqrt{\alpha^2 + \beta^2}}(\alpha x + \beta y + \gamma) \tag{4}$$

which renders depth a linear function of Y only (see figure 2):

$$z(x, y) = z(Y) = Y\sqrt{\alpha^2 + \beta^2} \tag{5}$$

Under this transformation, the time of travel integral becomes

$$T = \int_C \frac{ds(x, y)}{\sqrt{gz(x, y)}} = \int_C \left(\sqrt{\frac{1 + (\frac{dX}{dY})^2}{gY\sqrt{\alpha^2 + \beta^2}}} \right) dY \tag{6}$$

which has the same form as the classical brachistochrone problem. Minimizing this integral using the calculus of variations yields the cycloid equations:

$$(X_1 - X_0) = a(\theta - sin(\theta)) \tag{7}$$

$$(Y_1 - Y_0) = a(1 - cos(\theta)) \tag{8}$$

The cycloid path $C(a, \theta) \rightarrow C(X, Y) \rightarrow C(x, y)$ between any two points (x_1, y_1), (x_0, y_0) is found by forcing the condition $[\theta < \pi]$ in equations (7) and (8). The travel time to all points within each triangle are calculated by numerically integrating equation (6) along each of these paths.

Beginning at the source coordinates supplied to the program, which can be either a single point or a predefined polygon (to simulate fault planes), the program propagates the wave outward using the cycloid curves to calculate the travel time to any point within the mapped bathymetric triangle. Overall, the wave is propagated taking a hexagon (six triangles) at a time and spiraling the leading edge outward until either all the points within the defined region (excluding the land) are assigned a travel time or until the maximum allowable travel time is reached. Some overlap regions occur during the procedure because of the topological problem of covering a parallelogram with hexagons. Within these regions of recalculation, the shortest travel time is retained for each point.

RESULTS

The graphical output of the program is a travel time chart for a tsunami radiating outward from a point source (see Figures 3 and 4)—although a polygonal source may be used. These

charts span the Caribbean region: 10–22° N and 60.2–80° W. The convexity and spacing of the wavefronts gives us information about wave speed and sea depth simultaneously. The wide, highly convex wavefronts along the north side of the Greater Antilles Islands are indicative of the deep Puerto Rico Trench where faster waves would be expected, whereas the flat, uniform wavefronts running across the middle of the Caribbean indicate the relatively smooth uniform depth and wave speed of that area. The breakdown of linear wave theory and the limit of this program's usefulness is reached as the waves run into the shallow coastal areas. Two charts have been included here to demonstrate the two ways this program may be employed.

In the first chart (Figure 3), the source is placed at a point just east of Martinique, in the seismic gap area of high earthquake potential along the eastern edge of the Caribbean plate where one might expect a tsunamigenic earthquake to occur. This figure shows the time for such a wave to reach the rest of the Caribbean: 80 minutes to San Juan, Puerto Rico, 100 minutes to both Santo Domingo, in the Dominican Republic, and Caracas, Venezuela and 180 minutes to Kingston, Jamaica.

The second chart (Figure 4) demonstrates the second use of this program. Instead of supplying tsunami source coordinates, we can take advantage of the reversibility of linear wave theory by supplying the coordinates of various harbors and allowing the program to calculate travel times radiating outward from them to all points in the region. Each chart, corresponding to each harbor, can then be read in reverse, as it were. One could locate the tsunami's source coordinates and read off the travel time from, and therefore to, their harbor. This chart places the sink at Charlotte Amalie (US VI), a port historically susceptible to tsunami damage. Thus we may read off the travel times to the sink from points in the Caribbean: 40 minutes from San Juan, 70 minutes from Santo Domingo, 100 minutes from Caracas and 140 minutes from Kingston. As this is a preliminary report, we have not yet produced a complete series of these charts for general use, but as the improvements are implemented, we will include them in subsequent reports. These charts were generated as ASCII text files, originally designed for a line-printer. We are currently installing a graphical contouring routine to enable high quality plotting.

DISCUSSION

One limit on the data is the grid size. The most adaptable data set that we have obtained so far is the ETOPO5, with a grid resolution of 5 minutes. The first problem with this grid size is that in the Caribbean the data points are spaced approximately 9 km apart, creating an area of uncertainty of 81 square km—large enough to envelope entire islands the size of Saba and smaller. The second problem with grid size is the variations in depth which get smoothed over by the interpolation procedure—the smaller the grid, the more accurate the interpolation. The problem we have incorporating the NOS 15 second bathymetry is due to the program's requirement of a completed rectangular grid of depth data, which means that if land areas exist within the region, those negative depths must also be included in

the data even though the wave will not be propagated there. The data we have came to us in numerous irregular small patches and it forms a very irregular rectangular picture of the region In addition, we were only able to obtain hydrographic data and it therefore gives no indication of the land. Thus we must incorporate the patches into several large rectangles, determine the location of land areas to the required resolution, fill in those points with zeros or negative values, and then interpolate to the missing hydrographic points to fill out the grid. This procedure is currently underway.

Just how close to the harbor these travel time predictions are valid is determined by the breakdown of the linear long wave theory assumption. This theory is valid for values of the "Ursell parameter" [$U < 1.0$] (Murty, 1977). If we define depth, D, wavelength, λ, and amplitude, η, then we have:

$$U \equiv \frac{\eta \lambda^2}{D^3} \tag{9}$$

If we let the breakdown point occur at $U = 1.0$, solve for depth and plug-in typical values for the variables, we obtain a theoretical breakdown depth of:

$$D = \sqrt[3]{\frac{\eta \lambda^2}{U}} = \sqrt[3]{\frac{(0.3)(10^5)^2}{1.0}} \simeq 1400\ m \tag{10}$$

Thus at depths less than about fourteen hundred meters, the linear wave theory begins to break down and the wave speed will be slower than predicted. Therefore, the program will predict arrival times which are earlier than the observed waves. And for the purpose of tsunami hazard warning, the error is in the desirable direction. Exactly how much earlier the theory will predict for the wave's arrival is difficult to say since the breakdown of the linear wave theory forces a much more complicated analysis in which many more location specific parameters must be evaluated. This is the separation of the global propagation problem and the local run-up problem.

With the problem of the grid resolution in mind, one may wonder why the program uses the linear interpolation method of fitting a depth plane to three points instead of more sophisticated procedures. The advantage of the depth plane is that it allows the coordinate transformation to a system in which depth is a function of only one variable, which enables the brachistochrone analogy. Without this linear depth scenario, the cycloid equations and the calculus of variations would no longer guarantee the path of least time. Therefore we must sacrifice depth accuracy to achieve least time reliability.

The computation speed of the machine used to make the calculations places a limit on the minimum source distance from which one may obtain real time warnings. In the case of figures 3 and 4, our VAX took twenty minutes of cpu time to calculate the travel time grid and a few more minutes to produce the chart. Of course, faster and more dedicated machines could be used, as well as quicker plotting devices, but a certain minimum radius must be accounted for. Undoubtedly, this radius could be reduced below the breakdown point of the linear wave theory, the point at which one would want to turn to another model for the run-up.

CONCLUSIONS

As our interest in this project is the protection against the destruction wrought by tsunamis, perhaps by contributing to a real time early warning system in the Caribbean, we need to consider the practical uses of such a program as this. Unless a comprehensive early warning system, perhaps an extension of the THRUST system, is implemented for the entire region, this program would be best implemented to generate a series of travel time charts utilizing the reversibility feature, which in turn, can be used to give an approximation of the arrival time of a possible tsunami, once one is suspected to have been generated. One of the advantages to this method is the comprehensive nature of the resulting maps which show the travel time to every point in the region. These maps may be published and widely distributed to technologically poor regions.

If calculation speed is desired and one had a set of source and sink coordinates in mind, as in a real time situation for a specific harbor, then one may want to use a program which only considers travel from the source point to the harbor. A program utilizing the Grid Refinement Technique of Braddock (1969, 1971, 1979) would seem to be a good possibility for further work in this area.

If, as in the case of the Lisbon earthquake of 1755, we desire to know the travel time of a tsunami crossing the Atlantic, we would have to supply bathymetry for the entire rectangular region defined by the source (Lisbon) and the Caribbean. We are presently converting the ETOPO5 data for that calculation which may give us an opportunity for more extensive calibration.

Finally, the program is only capable of calculating travel times and localized wave velocities for the direct wave. No accounting is made for reflection, refraction, or diminution. It is also incapable of predicting energy transport or amplitudes, a direction which we may be exploring in the future.

ACKNOWLEDGEMENTS

I would like to thank the following people: Carl Kisslinger and Max Wyss for their support and advice on this work, Jim Lander for his enthusiasm for tsunami work, Pat Lockridge and the Geophysical Data Center for supplying the bathymetry and historical tsunami data, Masami Okada for generously allowing me to use his program and for his thoughtful explanations, and Paul Bodin and Arthur Rodgers for their editing suggestions. This work has been supported by a stipend from the Cooperative Institute for Research in Environmental Sciences (CIRES) and is continued with funding from the National Oceanic and Atmospheric Administration (NOAA).

References

Braddock, R. D. *Tsunami Propagation over Large Distances*, In *Tsunamis in the Pacific Ocean*(ed. Adams, William Mansfield) (East-West Center Press, Honolulu, 1969) pages 285–303, The International Symposium on Tsunamis, Sponsored by the International Union of Geodesy and Geophysics.

Braddock, R. D. (1971), *The Grid Refinement Technique*. Journal of Optimization Theory and Applications, *7*, 337–345.

Braddock, R. D. , G. Voss, and P. Doilibi *A New Method of Constructing Tsunami Ray Paths and Travel Time Charts*, In *Proceedings, Tsunami Symposium*, (Griffith University, Canberra, 1979) pages 241–262.

Jordan, T. (1975). *The Present-Day Motions of the Caribbean Plate*. Journal of Geophysical Research, *80*, 4433–4439.

Mallet, R. (1852). *Catalogue of Recorded Earthquakes*. Transactions, British Association for Advancement of Science. London.

McCann, W.R. , S.P. Nishenko, L.R. Sykes, and J. Krause (1979). *Seismic Gaps and Plate Tectonics: Seismic Potential for Major Boundaries*. Pageoph, *117*, 1082–1147.

Molnar, P. and L.R. Sykes (1969). *Tectonics of the Caribbean and Middle America Regions*. Geol. Soc. Amer. Bull., *80*, 1634–1684.

Murty, T.S. *Seismic Sea Waves: Tsunamis* (Department of Fisheries and the Environment, Ottawa, 1977) Bulletin of the Fisheries Research Board of Canada, Bulletin 198.

Reid, H. and S. Tabor (1919). *The Puerto Rico Earthquakes of October–November, 1918*. The Bulletin of the Seismological Society of America, *9*, 94–127.

Reid, H. F. and S. Taber (1920). *The Virgin Islands Earthquakes of 1867–1868*. The Bulletin of the Seismological Society of America, *10*, 9–30.

Sykes, L. R. , J. B. Kisslinger, L. House, J. N. Davies, and K. H. Jacob. *Rupture Zones & Repeat Times of Great Earthquakes Along the Alaska-Aleutian Arc 1784–1980*. In *Earthquake Prediction: An International Review*(eds. Simpson, David W. and Paul G. Richards) (American Geophysical Union, Washington, D.C., 1981) pages 73–79, Volume 4 of the Maurice Ewing Series.

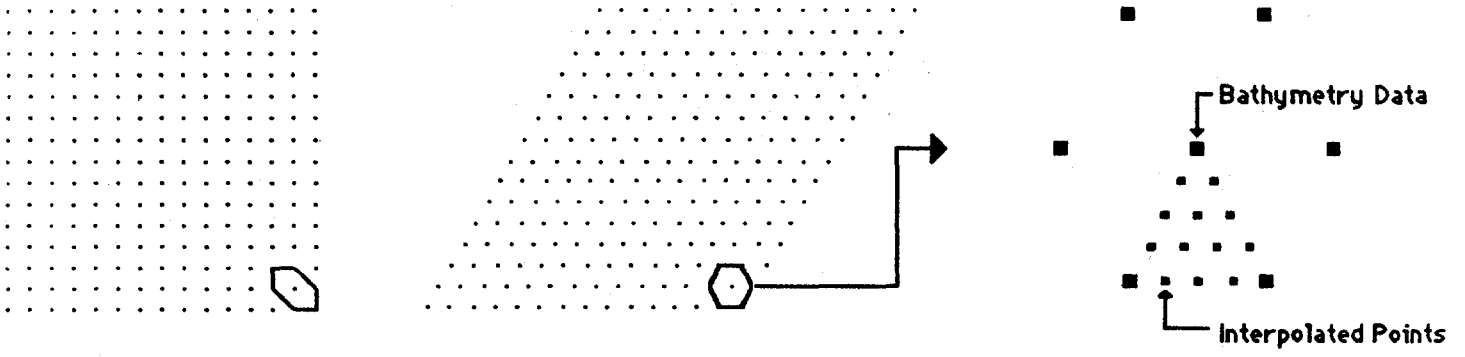

Fig. 1a Fig. 1b Fig. 1c

Figure 1: A rectangular bathymetry grid (a) is mapped into a 60–120 degree parallelogram (b). The parallelogram is then broken-down into hexagons made-up of six equilateral triangles (c). The three points of each triangle are used to fit a depth plane for interpolation to the twelve interior points.

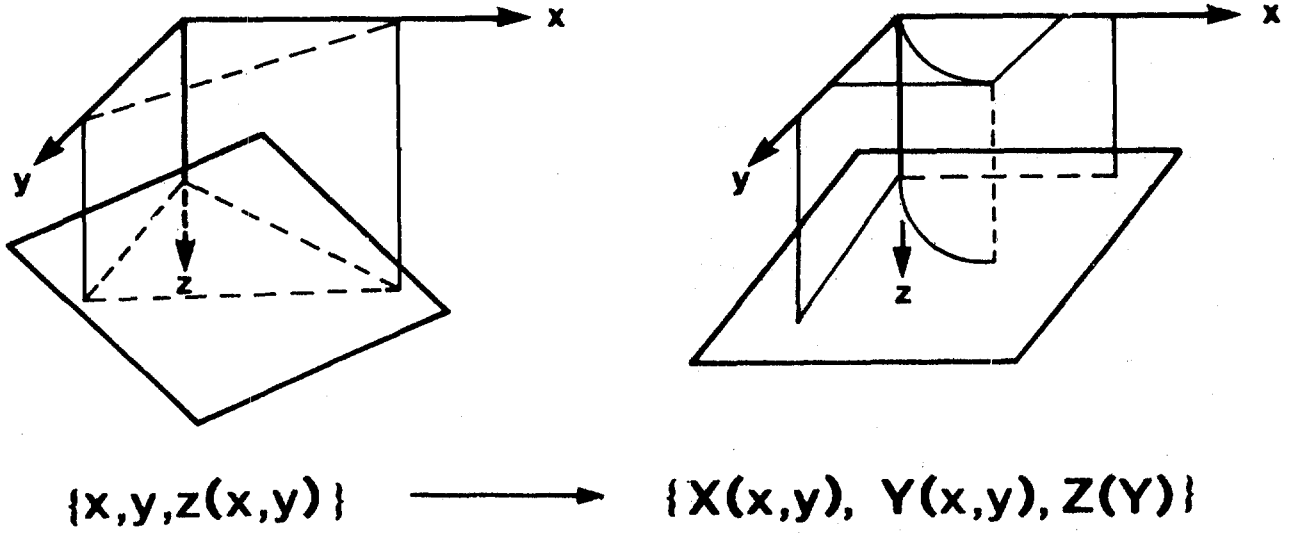

Figure 2: The fitted three-point depth plane fitted to the bathymetry triangle initially has an arbitrary orientation (a). In (b) a coordinate transformation is made to establish depth as a function of only one variable for the cycloid curve fit 'C'.

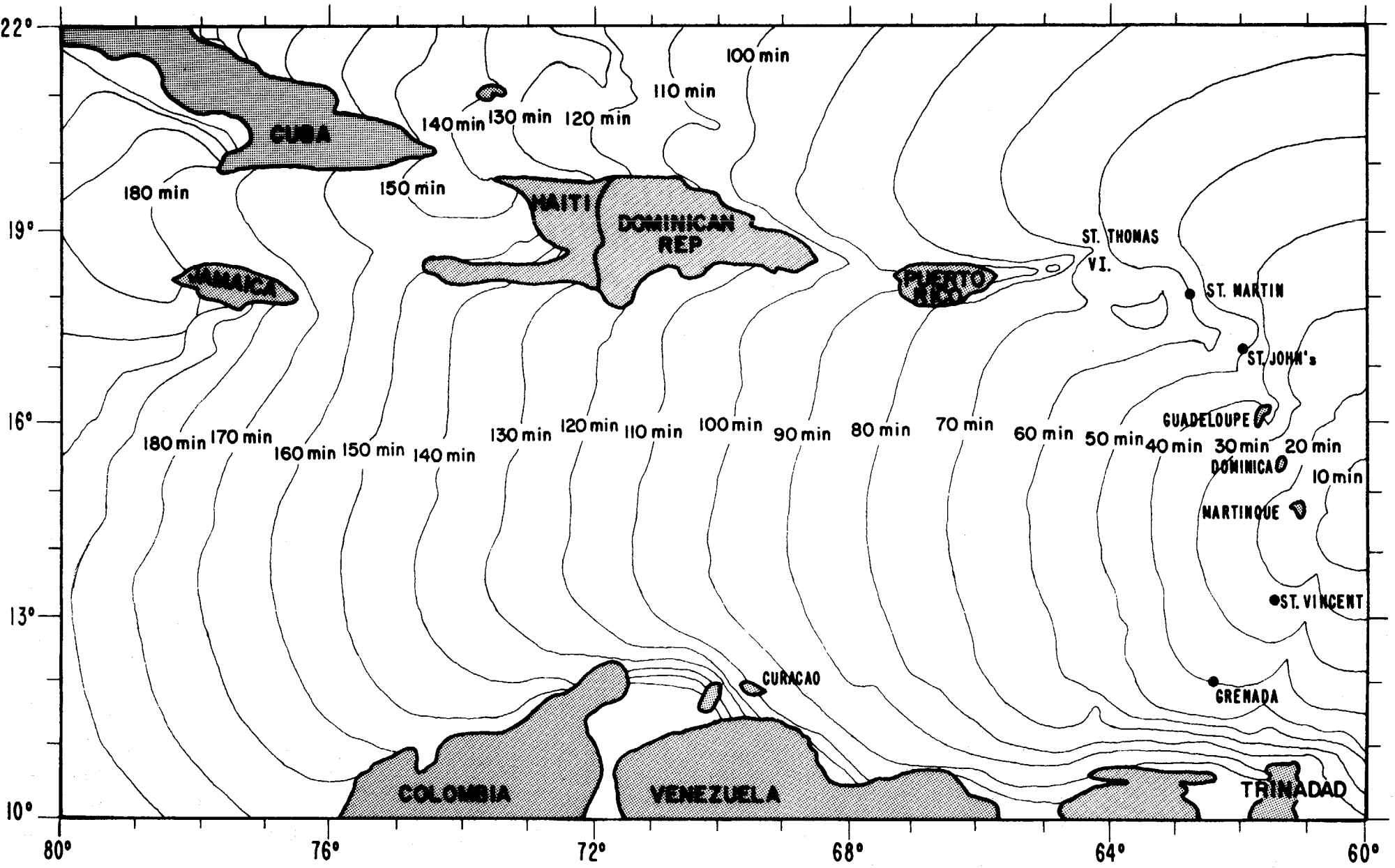

Figure 3: This chart shows the progress of a tsunami generated along the underthrusting outer east edge of the Caribbean plate. This is an example of using the program in the forward direction -- to model a tsunami from its source.

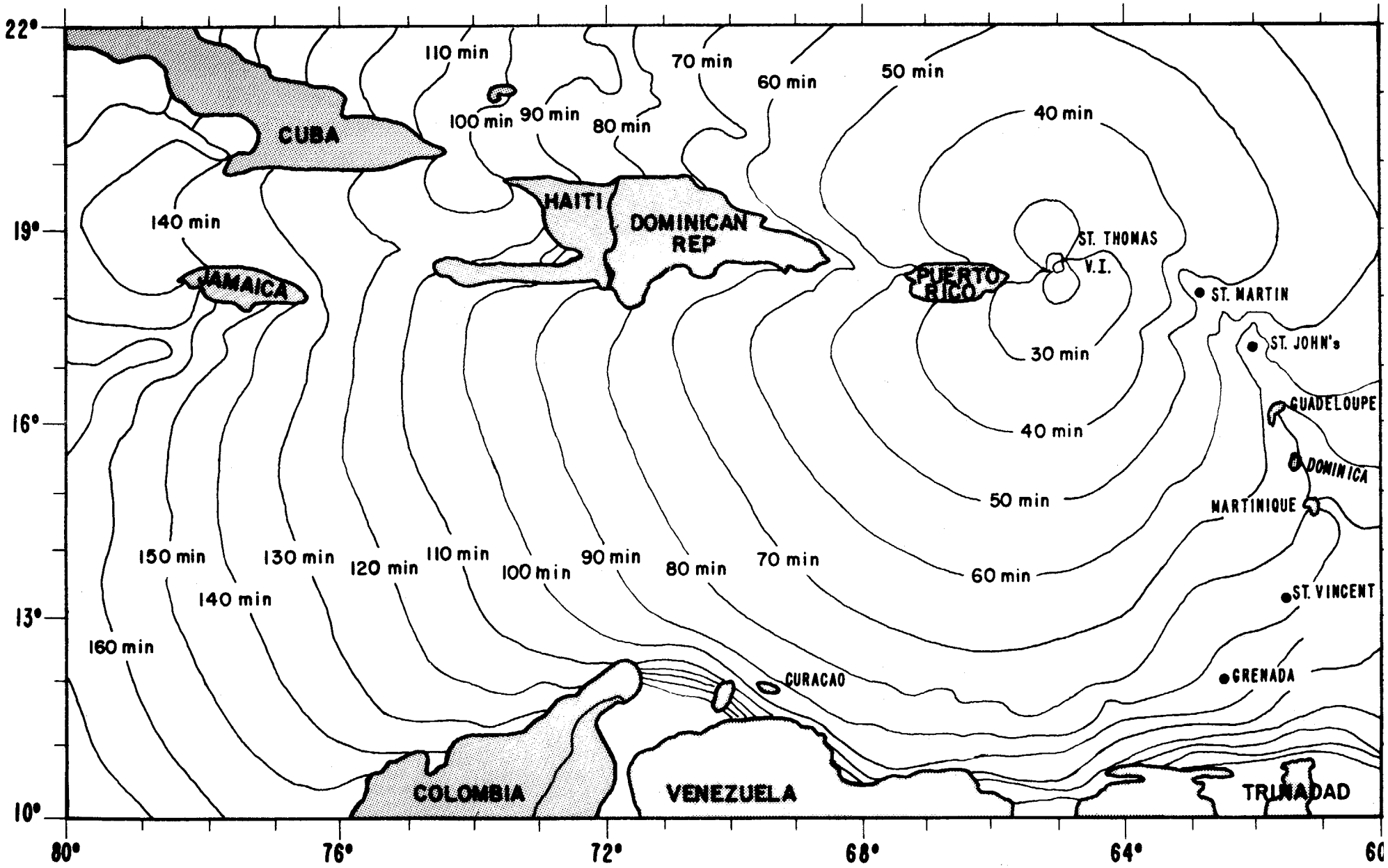

Figure 4: A travel-time chart for the Caribbean showing ten-minute wavefronts for a tsunami "generated" at Charlotte Amalie (US VI). This is an example of choosing a specific harbor as a tsunami sink.

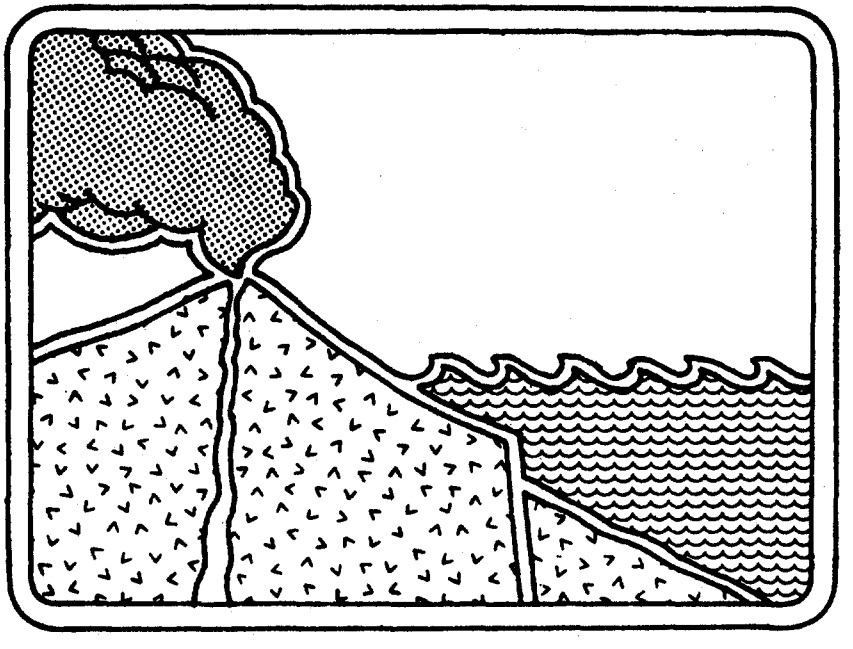

NUMERICAL TSUNAMI FLOODING STUDY - I

Charles L. Mader
Joint Institute for Marine and Atmospheric Research
University of Hawaii, Honolulu, HI., U.S.A.

ABSTRACT

The *SWAN* code solves the nonlinear, shallow water, long wave equations including the effects of friction and flooding. The *SWAN* code was used to study the effect of tsunami wave period, amplitude, bottom slope angle and friction on tsunami shoaling and flooding. A 3 meter high tsunami wave was propagated in 12 meter deep water and then interacted with slopes between 0.25 and 5.0 percent. Waves were studied with periods of 225 to 3600 seconds. The effect of bottom friction was examined using De Chezy coefficients ranging from 10 (large amount of friction) to infinity (no friction).

Also studied was a one meter high tsumani wave propagating in 4550 meter deep water and then interacting with slopes between 0.75 and 13.5 percent. Wave periods of 250 to 2500 seconds were studied. Both the *SWAN* and *ZUNI* code which solves the incompressible Navier-Stokes equations were used in the study.

The study showed higher wave shoaling and flooding for steeper slopes, for longer periods, and from deeper water. The shallow water waves shoal higher, steeper and faster than the Navier-Stokes waves. The differences increase as the periods become shorter and the slopes less steep with large differences for periods less than 500 seconds and slopes less than 2 percent.

Introduction

The magnitude of the tsunami hazard at any land site depends upon the expected extent of flooding of the land by tsunamis at the site, the expected water velocities and the exposure of persons and property within the potential flood zone. The development of numerical models to describe tsunami wave interaction with complicated topography such as bays or harbors and the resulting flooding has advanced to the stage where they are useful tools for determining the tsunami hazard in local regions.

NOAA is developing a Tsunami Inundation Project similar to the NOAA Storm Surge Program. The project is to set national standards for tsunami inundation models designed to mitigate the tsunami hazard to U.S. coastlines. The relative importance of the characteristics of the tsunami and the topography in and between the available numerical models has not been established.

The characterization of the tsunami flooding problem is a large and continuing effort. In this paper we describe the first results of our parameteric study of numerical tsunami models. The most common model used to describe tsunami flooding is the nonlinear, shallow water, long wave model. A severe limitation to such models is called the "long wave paradox". The long wave model results in waves that become steeper as they move down a flat channel, that are too steep and move too fast as they shoal and therefore break too early. The problem is more serious as the distance and time of interest increases. Although the "long wave paradox" is a limitation on the accuracy of the results, the model can be very useful and inexpensive if applied cautiously to appropriate problems. Only recently have flooding capabilities been developed in the numerical models using the shallow water approximation, so characterization remains to be accomplished as does comparision with more realistic models.

A more realistic description of water waves and flooding uses the Navier-Stokes equations. An early study of the shoaling and flooding using the Navier-Stokes equations is described in reference 1. In this paper we will extend that study to examine the various parameters in more detail and in particular to compare with shallow water flooding results.

The Shallow Water Numerical Model

The tsunami waves and their interaction with slopes of various steepness were numerically modeled using the *SWAN* code and the *ZUNI* code. The *SWAN* code solves the incompressible, shallow water, long wave equations. It is described in detail in the monograph *Numerical Modeling of Water Waves* [1] .

The incompressible, shallow water, long wave equations solved by the *SWAN* code are

$$\frac{\partial U_x}{\partial t} + U_x\frac{\partial U_x}{\partial x} + U_y\frac{\partial U_x}{\partial y} + g\frac{\partial H}{\partial x} = FU_y + F^{(x)} - g\frac{U_x(U_x^2+U_y^2)^{1/2}}{C^2(D+H-R)} ,$$

$$\frac{\partial U_y}{\partial t} + U_x\frac{\partial U_y}{\partial x} + U_y\frac{\partial U_y}{\partial y} + g\frac{\partial H}{\partial y} = -FU_x + F^{(y)} - g\frac{U_y(U_x^2+U_y^2)^{1/2}}{C^2(D+H-R)} ,$$

$$\frac{\partial H}{\partial t} + \frac{\partial(D+H-R)U_x}{\partial x} + \frac{\partial(D+H-R)U_y}{\partial y} - \frac{\partial R}{\partial t} = 0 ,$$

where U_x is velocity in x direction, U_y is velocity in y direction, g is gravitational acceleration, t is time, H is wave height above mean water level, R is bottom motion, F is Coriolis parameter, C is coefficient of DeChezy for bottom friction, $F^{(x)}, F^{(y)}$ are forcing functions of wind stress in x and y direction, and D is depth.

Flooding was described using positive values for depths below normal water level and negative values for elevations above normal water level. Only positive values of the $(D + H)$ terms in the above equations were permitted. This method results in both flooding and receeding surfaces being described by the *SWAN* code.

The *SWAN* code has been used to study the interaction of tsunami waves with continental slopes and shelves, as described in reference 2. Comparison with two-dimensional Navier-Stokes calculations of the same problems showed similar results, except for short wavelength tsunamis. The flooding permitted in the shallow water model is investigated in more detail in this paper.

The *SWAN* code was used to model the effects of tides on the Musi-Upang estuaries, South Sumatra, Indonesia, by Safwan Hadi.[3] The computed tide and water discharge were in good agreement with experimental data.

The *SWAN* code was used to model the large waves that were observed to occur inside Waianae harbor under high surf conditions in reference 4. These waves have broken moorings of boats and sent waves up the boat-loading ramps into the parking lot. The numerical model was able to reproduce actual wave measurements. The *SWAN* code was used to evaluate various proposals for decreasing the amplitude of the waves inside the harbor. From the calculated results, it was determined that a significant decrease of the waves inside the harbor could be achieved by decreasing the harbor entrance depth.

The effect of the shape of a harbor cut through a reef on mitigating waves from the deep ocean was studied using the *SWAN* code in reference 5. It was concluded that a significant amount of the wave energy is dissipated over the reef regardless of the design of the harbor. The reef decreased the wave height by a factor of 3. The wave height at the shore can be further decreased by another factor of 2 by a "V"-shaped or parabolic bottom design.

Other examples of applications of the *SWAN* code are presented in reference 6. They include the wave motion resulting from tsunami waves interacting with a circular and triangular island surrounded by a 1/15 continental slope and from surface deformations in the ocean surface near the island. The effects of a surface deformation in the Sea of Japan similar to that of the May 1983 tsunami was modeled.

The *SWAN* code was used to model the effect of wind and tsunami waves on Maunalua Bay, Oahu as described in reference 7. The model reproduced the observed wave behavior at various locations in the bay for a 1.2 meter south swell with a 15 second period. The code was used to model the interaction with Maunalua Bay of waves outside the bay having periods of 15, 30, 60 seconds and a tsunami wave with a 15 minute period. Wave amplitudes of 0.3 to 1.8 meters were considered with tides from mean lower low water to high tide (a 0.55 meter range). The 15 minute period tsunami wave doubled in amplitude as it passed over the bay and was highest at high tide. Severe flooding in the regions near the shore line was predicted. The calculated wave behavior at any location in the bay was a strong function of the entire bay with a complicated and time varying pattern of wave reflections and interactions.

The interaction of a tsunami wave with a site of well documented topography on the South Kohala Coast of the Island of Hawaii was described in reference 8. The tsunami wave was calculated to flood the land to the 3 meter level and inundate the land between 90 and 120

meters from the shoreline. These results agree with the results obtained using the procedures developed and applied for flood insurance purposes by the U. S. Army Corps of Engineers and the recent JIMAR study at the University of Hawaii [9] of tsunami evacuation zones for the region.

The Navier-Stokes Numerical Model

The two-dimensional time dependent Navier-Stokes equations for incompressible flow solved by the *ZUNI* code are

$$\frac{\partial U_x}{\partial x} + \frac{\partial U_y}{\partial y} = 0 ,$$

$$\frac{\partial U_x}{\partial t} + U_x\left(\frac{\partial U_x}{\partial x}\right) + U_y\left(\frac{\partial U_x}{\partial y}\right) = -\frac{1}{\rho_o}\frac{\partial P}{\partial x} + g_x + \frac{\mu}{\rho_o}\left(\frac{\partial^2 U_x}{\partial x^2} + \frac{\partial^2 U_x}{\partial x \partial y}\right) ,$$

$$\frac{\partial U_y}{\partial t} + U_x\left(\frac{\partial U_y}{\partial x}\right) + U_y\left(\frac{\partial U_y}{\partial y}\right) = -\frac{1}{\rho_o}\frac{\partial P}{\partial y} + g_y + \frac{\mu}{\rho_o}\left(\frac{\partial^2 U_y}{\partial y \partial x} + \frac{\partial^2 U_y}{\partial y^2}\right)$$

where P is pressure and μ is the viscosity coefficient.

A partial cell treatment that allows a rigid free slip obstacle to be placed through cell diagonals is included. The desired boundary slope is obtained by choosing the appropriate aspect ratio for the cells of the mesh. Thus, the numerical technique can be used to calculate wave run-up on exposed beaches in addition to submerged beaches. The details of the calculational procedure are described in reference 1.

The detailed Navier-Stokes numerical simulation of gravity waves that resemble the profile of actual tsunami waves was first achieved in reference 2. The interaction of tsunami waves with slopes that resembled the continental slope and shelf was simulated. Wave heights were calculated to increase by a factor of 4 as they shoaled up a 6.66 percent continental slope.

The *ZUNI* code was used to model the effect of submerged barriers on waves as described in references 1 and 2. The calculated transmission coefficients (ratio of wave height inside to height outside barrier) from experimental underwater barrier data were reproduced by the numerical model. Underwater barriers reflect significant amounts of the tsunami energy approaching a bay or harbor.

Water waves generated by explosions which produce bubbles underwater and cavities in the water surface have been described using the *ZUNI* code in references 1 and 2. The experimentally observed waves generated by cavities were deep water waves which were reproduced using the *ZUNI* code but not by the *SWAN* code.

The interaction of waves with submerged barriers and explosively generated water waves can not be described using the shallow water model since significant features of the flow are characteristic of deep water waves.

The tsunami of November 29, 1975 on the island of Hawaii has been investigated using the *SOLA* code [1] that solves the three-dimensional, incompressible Navier-Stokes equations. Sources investigated were landslides and an uplift or drop of the ocean floor. The observed wave features

were not described by the landslide model, but were reproduced by the uplift model as described in references 10 and 11.

Application of the *SWAN* Model

A 3 meter half-height tsunami wave of various periods was propagated in 12 meter deep water and then interacted with slopes of various steepness. The calculations were performed on an IBM PS/2 Model 80 computer using a special version of the *SWAN* code that includes flooding and MCGRAPH graphics for the OS/2 operating system. A calculation required up to 2 hours of computer time for problems with a mesh of 500 by 4 cells and 2,200 cycles.

The wave height in meters as a function distance is shown in Figure 1 at various times for a tsunami Airy wave with a 900 second period and a 3 meter half-height traveling 3000 meters in 12 meter deep water before it interacted with a frictionless 1 percent slope. The space resolution in the numerical model grid was 10 meters with 300 cells to the bottom edge of the slope, 120 cells on the slope below and 80 cells above the water surface. The calculations were performed at 0.5 second intervals. The peak wave height was 6.7 meters, the runup wave height was 6.0 meters and the inundation limit was 600 meters. The steepness of the slope was changed by changing the space resolution and the time step. The wave period was changed assuming that the tsunami was a shallow water Airy wave. The results are shown in Table 1 and Figures 2 thru 5. The numerical model grid described is satisfactory for the cases studied giving runup and inundation values that are independent of space, time and geometry resolution. The grid model becomes less accurate for steeper slopes and longer wave length waves. The longer wave length waves need longer distances and times for the shoaling to occur; otherwise the calculated runup and inundation will be grid size dependent, decreasing with decreasing distance to the bottom edge of the slope.

The effect of the steepness of a frictionless slope on the runup height and inundation limit is shown in Figure 2 for a tsunami wave with a 3 meter half-height and a 900 second period in 12 meters of water. As shown in Figure 1, the highest shoaling wave height does not necessarly occur at the front of the wave. The difference between the height at the front of the wave and the peak wave height increases as the slope becomes steeper, with the maximum difference occuring for slopes larger than 1.5 percent. As shown in Figure 2 the runup height decreases and the inundation limit increases with decreasing slope angle.

Also shown in Figure 2 is the predicted runup height for the Bretschneider model without friction. The Bretschneider model results in smaller runup than *SWAN* for slopes greater than 1 percent. The current engineering method for estimating maximum probable tsunami inundation zones is to use historical inputs to provide tsunami wave heights as a function of frequency of occurrence and then to use the Bretschneider model described in reference 12 to calculate the runup on the shore at selected sites. The Bretschneider model as it is normally used includes surface roughness. The roughness parameters have been calibrated to reproduce observed runups. The Bretschneider model is independent of wave period and the only slope effect is from the friction.

The effect of wave period and frictionless slope steepness on tsunami flooding is shown in Figure 3. The maximum runup height is obtained for short period waves interacting with steep slopes, while the maximum inundation occurs for 1000 second waves on gentler slopes.

The effect of friction on tsunami flooding of 1 and 2 percent slopes is shown in Figures 4 and 5. The effect of increasing friction (decreasing DeChezy friction constant) is small on the peak

height and becomes larger on the runup height as the slope decreases. In the Bretschneider model the surface roughness is described using a Manning "n" where 0.04 corresponds to a roughness characteristic of grass or small rocks and 0.03 to a roughness of many trees, large boulders or high grass. The De Chezy friction coefficient is related to Manning "n" by the depth to the 1/6 power. While not directly comparable, for depths in this study a De Chezy friction coefficient of 50 results in about the same friction effect as a Manning "n" in the 0.03-0.04 range.

Application of the *ZUNI* Model

A 1 meter high tsunami wave of various periods was propagated in 4550 meter deep water and then it interacted with frictionless slopes of various steepness. These results are an extension of those described in references 1 and 2. The calculations were performed on an IBM PS/2 Model 80 computer using a special version of the *ZUNI* code that includes flooding and MCGRAPH graphics for the OS/2 operating system. Calculations were also performed using a CRAY computer.

The geometry of the flooding calculation is shown in Figure 6 for a 1/15 or 6.66 percent slope. The calculations for this geometry were performed with 15 cells in the Y or depth direction and 68 cells in the X or distance direction. The cells were rectangles 450 meters high in the Y direction and 6750 meters long in the X direction. The time increment was 3 seconds. The water level was placed at 4550 meters or 50 meters up into the eleventh cell. The viscosity coefficient used was 0.02 poise, a value representative of the actual viscosity for water. The viscosity did not significantly affect the results. The slope in a *ZUNI* calculation is determined by the diagonal through the cell as discussed in the numerical methods section. A 6.66 percent slope results in a cell aspect ratio of 1 to 15 and a 4.0 percent slope an aspect ratio of 1 to 25. Numerical errors increase with increasing aspect ratio to unacceptable levels for 1 to 50 and greater ratios. Another method of changing the slope is to keep the width and aspect ratio constant and change the depth of the calculation. This permits slopes from 12.48 to 0.75 percent to be studied; however if the period is kept constant, the other wave parameters change as shown in Table 3.

The slope study was performed using both methods to change the slope with the results shown in table 2 and figure 7. The general features of the calculated runup as a function of slope are the same for the *ZUNI* and *SWAN* models as shown in figures 2 and 7. The resolution of the *ZUNI* calculation is inadequate to resolve the peak from the runup height. The *ZUNI* calculation permits us to realistically calculate wave interactions after the first wave interacts with the slope and to obtain rundown and runup for later waves. This is important because the largest runup both observed and in these calculations is the second or third wave. The interaction of the reflected waves with the later waves often results in the second or third runup being much different than the first runup. The magnitude and direction of the effect depends upon both the slope and the wave period as shown in table 2. To perform these calculations, the source of the wave must be far removed from the slope in order to correctly follow the interaction of the incoming and reflected waves for several waves. A longer wave period needs a larger distance to run and requires more time for the multiple wave interactions. This results in large computing meshes and long running times for the long period tsunamis. Since they also result in the greatest flooding, they are also of the most interest.

The effect of wave period was investigated for a 1 meter half-height wave at 4550 meters interacting with a 6.66 percent slope and at 1011 meters depth with a 1.48 percent slope. The results of the study of wave period and slope are shown in table 2 and figure 8. Also shown

in figure 8 are the *SWAN* runup heights as a function of period for the first wave. To obtain adequate resolution in the *SWAN* calculation, a much smaller mesh is required than in the *ZUNI* calculation. This is a result of the particle surface following treatment in the *ZUNI* calculation which resolves the surface in each cell. The *SWAN* calculations were performed using a 780 cell long mesh, a mesh width of 500 meters and a time step of 0.3 second. The 4500 deep bottom was 250 km long (500 cells) to the edge of the 5 percent shelf formed by 91 km (180 cells) below and 50 km (100) cells above the water surface. Calculations were also performed using a mesh width of 250 meters and a 1560 cell long mesh.

As shown in table 2 and Figure 8, the shallow water waves flood higher for the first wave than the Navier-Stokes waves. The differences increase as the periods become shorter and the slopes less steep, with large differences for periods less than 500 seconds and slopes less than 2 percent. For higher period waves, the second wave is as much as a third larger than the first wave. The second wave is also larger than the shallow water first wave for wave periods greater than 500 seconds.

Conclusions

The effect of tsunami wave period, amplitude, bottom slope angle and friction on tsunami shoaling and flooding has been investigated using a shallow water and a Navier-Stokes model.

The study shows higher wave shoaling and flooding for waves interacting with steeper slopes, for waves with longer periods and for waves from deeper water. The shallow water waves shoal higher, steeper and faster than the Navier-Stokes waves. The differences increase as the periods become shorter and slopes less steep with large difference for periods less than 500 seconds and slopes less than 2 percent.

The interaction of the reflected first wave with the later waves often results in the second or third runup being much different than the first runup. The magnitude and direction of the effect depends upon both the slope and the wave period. For higher period waves, the second wave is as much as a third larger than the first wave. Since the shallow water model distorts the shoaled and reflected wave, the wave interaction and resulting second and third runups are inaccurately modeled. This needs to be evaluated in future parameteric studies.

The effect of friction was investigated only for the shallow water model. It is the largest unknown factor in evaluating tsunami flooding. The Navier-Stokes model used does not have a treatment for friction. The development and evaluation of better friction models is probably the most important remaining tsunami flooding problem.

Only part of the parameteric region of interest for tsunami flooding has been investigated, particularly for the Navier-Stokes model. Since three-dimensional Navier-Stokes solutions to tsunami flooding problems currently have limited practical application, most tsunami flooding studies will need to be performed using the shallow water model. These studies permit us to determine the parameteric region where the shallow water model can be useful.

Acknowledgments

The author gratefully acknowledges the contributions of G. D. Curtis, D. W. Moore and H. G. Loomis of the University of Hawaii, Z. Kowalik of the University of Alaska, T. S. Murty of the Institute of Ocean Sciences, and E. N. Bernard of the Pacific Marine Environmental Laboratory.

References

1. Charles L. Mader *Numerical Modeling of Water Waves,* University of California Press, Berkeley, California (1988).
2. Charles L. Mader, "Numerical Simulation of Tsunamis," Journal of Physical Oceanography, Vol. 5, pp. 75–82 (1975).
3. Safwan Hadi, "A Numerical Tidal Model of Musi-Upang Estuaries." A dissertation submitted to Oceanography Department of University of Hawaii (1985).
4. Charles L. Mader and Sharon Lukas, "Numerical Modeling of Waianae Harbor," Aha Hulikoa Hawaiian Winter Workshop Proceedings (January 1985).
5. Charles L. Mader, Martin Vitousek, and Sharon Lukas, "Numerical Modeling of Atoll Reef Harbors," Proceedings of the International Symposium on Natural and Man-Made Hazards, Rimouski (1986).
6. Charles L. Mader and Sharon Lukas, "*SWAN* – A Shallow Water, Long Wave Code: Applications to Tsunami Models," Joint Institute for Marine and Atmospheric Research report JIMAR 85–077 (1985).
7. "Oahu Intraisland Ferry System - Draft Environmental Impact Statement," State Department of Transportation, Harbors Division (1988).
8. Charles L. Mader "Modeling Tsunami Flooding," Proceedings of the Pacific Congress on Marine Science and Technology - PACON 90 (1990).
9. George D. Curtis and Mark Smaalders, "A Methodology for Developing Tsunami Evacuation Zones," Proceedings of International Tsunami Symposium 89 (1989).
10. Charles L. Mader, Robert E. Tangora, and B. D. Nichols, "A Model of the 1975 Hawaii Tsunami," Natural Science of Hazards Vol 1, C1-8 (1982).
11. Charles L. Mader, "A Landslide Model for the 1975 Hawaii Tsunami," Science of Tsunami Hazards, Vol 2, 71-78 (1984).
12. C. L. Bretschneider and P. G. Wybro, "Tsunami Inundation Prediction," Proceedings of 15th Coastal Engineering Conference (1976).

TABLE 1

SWAN Shallow Water Flooding Study

Slope Percent	Period Seconds	DeChezy C	Peak Ht. meters	Runup Ht. meters	Inundation Limit meters
	Initially 3 m Wave at 12 m Depth				
4.0	900.	0.0	6.8	6.3	160
2.0	900.	0.0	7.0	6.4	330
1.0	900.	0.0	6.7	6.0	600
0.5	900.	0.0	5.0	4.7	1000
0.25	900.	0.0	3.7	3.2	1300
1.0	1570.	0.0	7.2	6.3	600
1.0	450.	0.0	5.2	4.8	500
1.0	225.	0.0	3.6	3.2	350
2.0	1800.	0.0	6.0	5.6	280
2.0	450.	0.0	6.8	6.0	300
2.0	225.	0.0	5.0	4.8	250
4.0	450.	0.0	7.0	6.4	160
4.0	225.	0.0	6.6	6.0	160
2.0	900.	10.0	4.8	0.5	30
2.0	900.	20.0	5.8	1.8	100
2.0	900.	30.0	6.4	3.0	160
2.0	900.	50.0	6.6	5.2	280
1.0	900.	10.0	4.2	0.4	40
1.0	900.	15.0	5.0	0.8	80
1.0	900.	25.0	6.0	1.6	160
1.0	900.	40.0	6.5	2.8	300
1.0	900.	50.0	6.5	3.8	390
1.0	900.	60.0	6.5	4.4	440
100.	3600.	0.0	4.8	4.8	
100.	900.	0.0	6.1	6.1	
100.	225.	0.0	6.5	6.5	
	Initially 1 m Wave at 4550 m Depth				
5.0	2666.	0.0		3.5	
5.0	1999.	0.0		3.7	
5.0	1666.	0.0		4.0	
5.0	1333.	0.0		4.5	
5.0	999.	0.0		5.5	
5.0	666.	0.0		6.5	
5.0	330.	0.0		7.7	

TABLE 2

***ZUNI* Navier-Stokes Flooding Study**

Slope Percent	Period Seconds	1st-Peak meters	1st-Trough meters	2nd-Peak meters	2nd-Trough meters
Period Study for 1 m Wave at 4550 m Depth					
6.66	1333.	+3.2	-3.2	+4.1	-4.1
6.66	900.	+3.0	-4.0	+4.1	
6.66	500.	+1.9	-2.9	+2.9	-2.9
6.66	250.	+0.9	-0.5	+0.25	-0.1
Period Study for 1 m Wave at 1011 m Depth					
1.48	2500.	+2.8	-3.3	+3.8	
1.48	1700.	+2.5	-3.7	+3.6	-3.2
1.48	1333.	+2.1	-3.6	+3.2	-3.3
1.48	900.	+1.5	-2.0	+2.0	
1.48	500.	+0.8	-0.3	+0.3	
Slope Study, Slope Width Varied, 4550 m Depth					
10.0	1333.	+3.0	-3.2	+3.2	
6.6	1333.	+3.2	-3.9	+4.1	-4.1
4.0	1333.	+2.9	-4.0	+3.9	-3.8
Slope Study, Depth Varied, Slope Width Constant					
13.48	1333.	+3.2	-3.3	+3.5	-3.0
6.66	1333.	+3.2	-3.9	+4.1	-4.1
2.96	1333.	+2.9	-3.9	+3.85	
2.22	1333.	+2.8	-3.8	+3.8	-3.7
1.48	1333.	+2.1	-3.6	+3.2	-3.3
0.74	1333.	+1.1	-1.9	+2.8	

TABLE 3

A 1333 Sec Tsunami Wave with Fixed Slope Width

Slope Percent	Period Seconds	Depth meters	Velocity m/sec	Length Slope km	Width km
13.48	1333.	9100.	299.	398.	68.25
6.66	1333.	4550.	210.	280.	68.25
2.96	1333.	2022.	141.	188.	68.25
2.22	1333.	1517.	122.	163.	68.25
1.48	1333.	1011.	99.	132.	68.25
0.74	1333.	505.	70.	93.	68.25

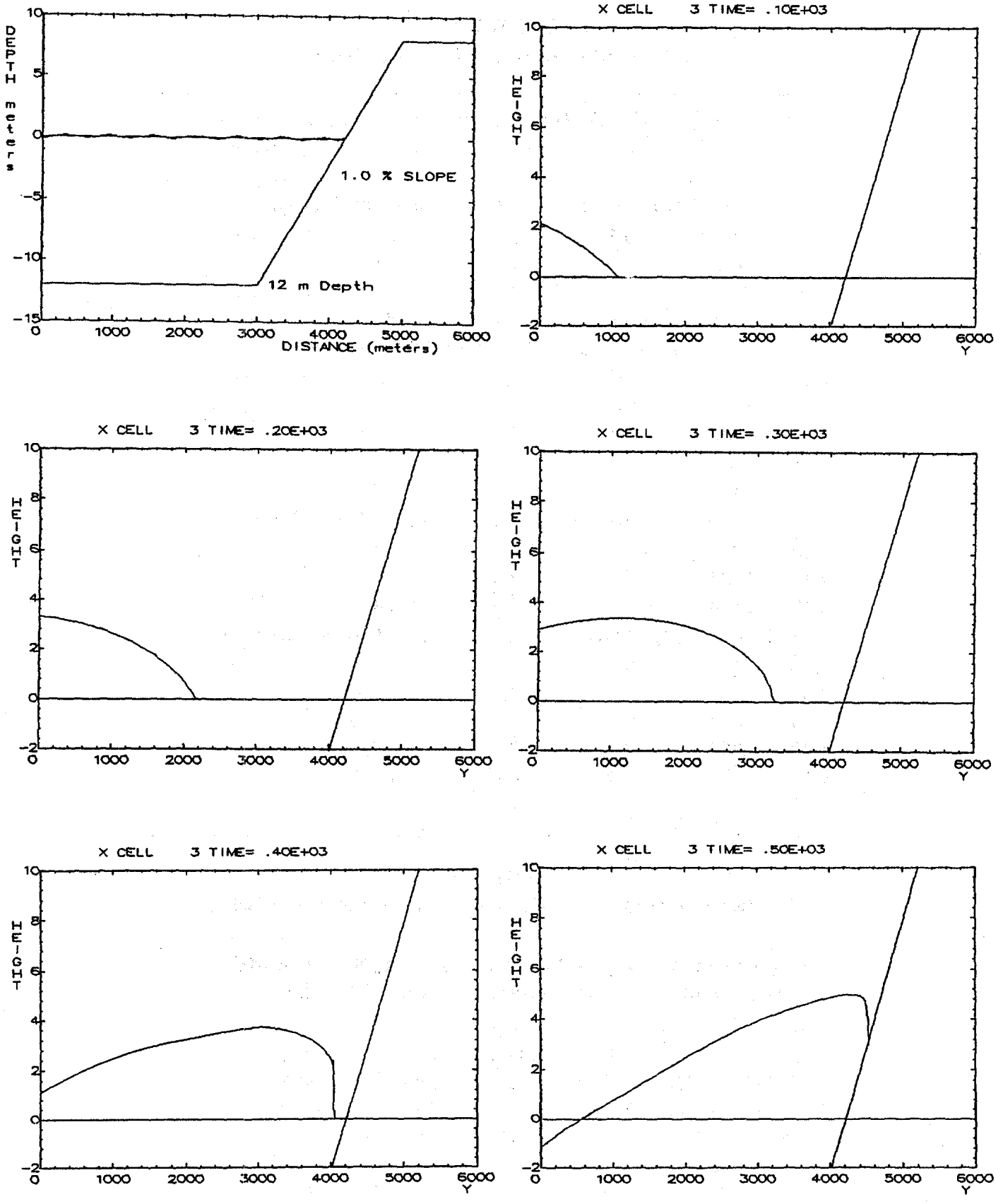

Fig 1. Initial geometry and interaction of a 900 second period, 3 meter half-height tsunami in 12 meters of water with a 1 percent slope at various times.

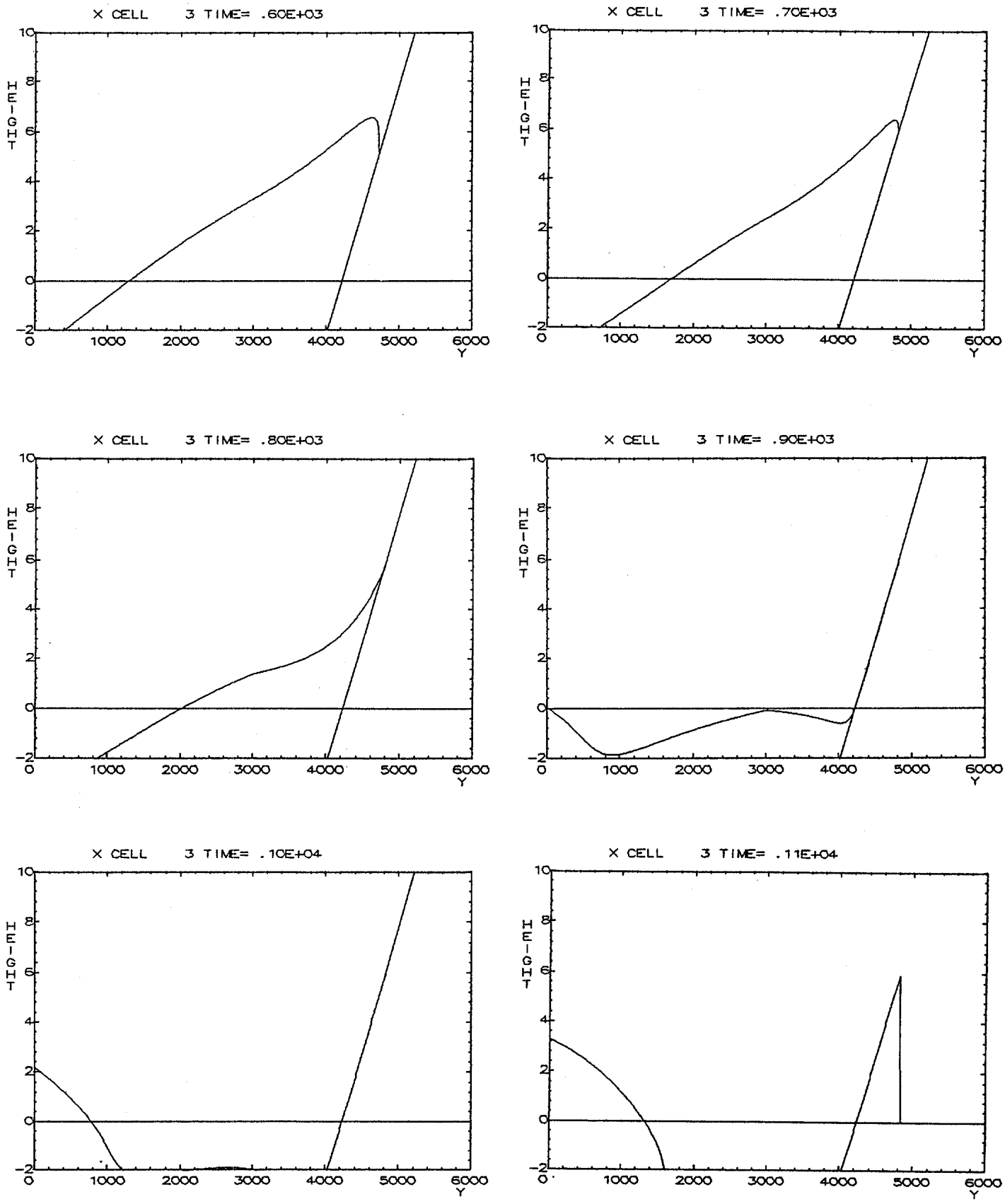

Fig 1. (Part 2.) The last figure shows the maximum extent of flooding by the first wave.

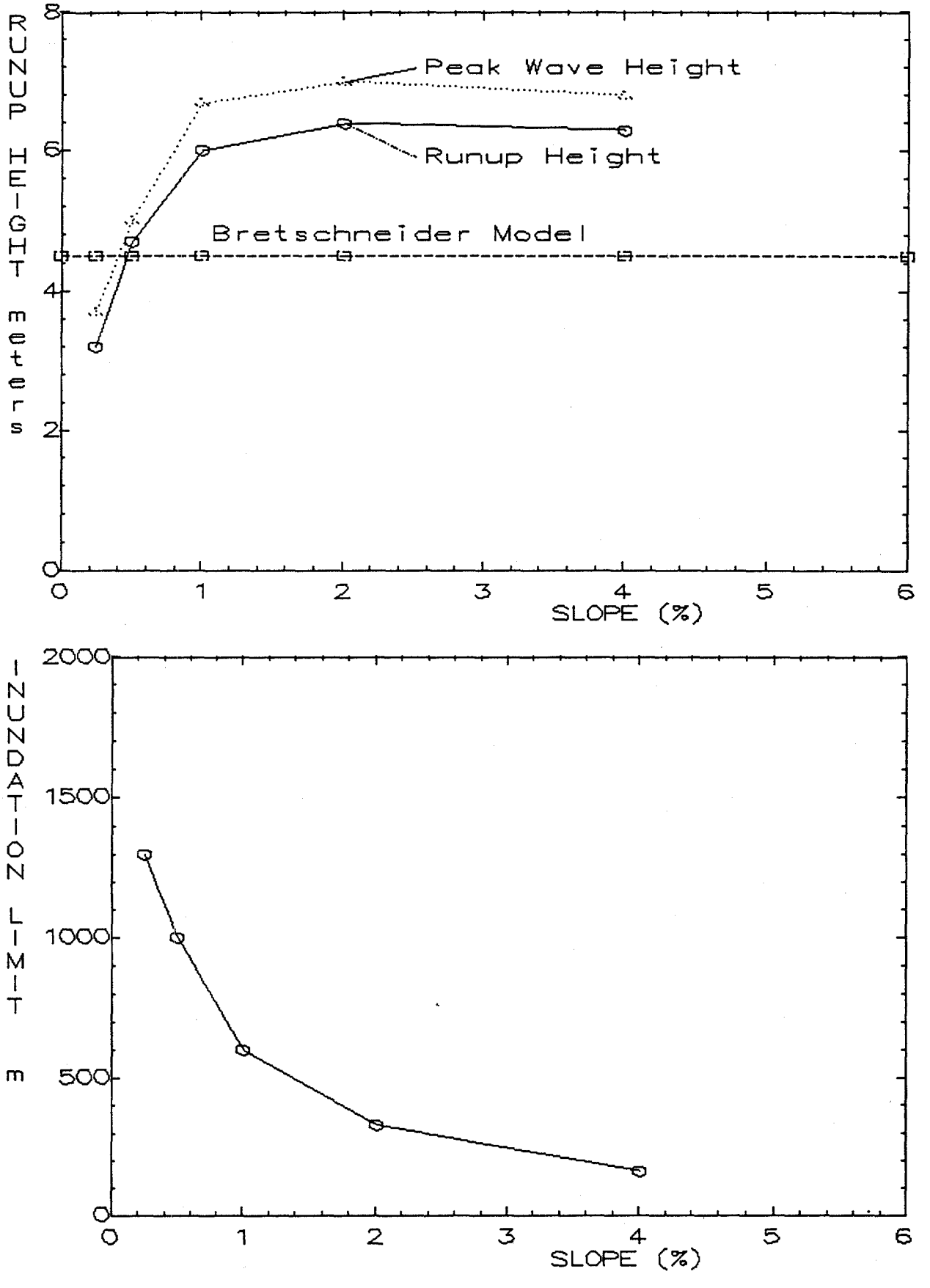

Fig. 2. Slope vs flooding by a 900 sec, 3 m high SWAN tsunami.

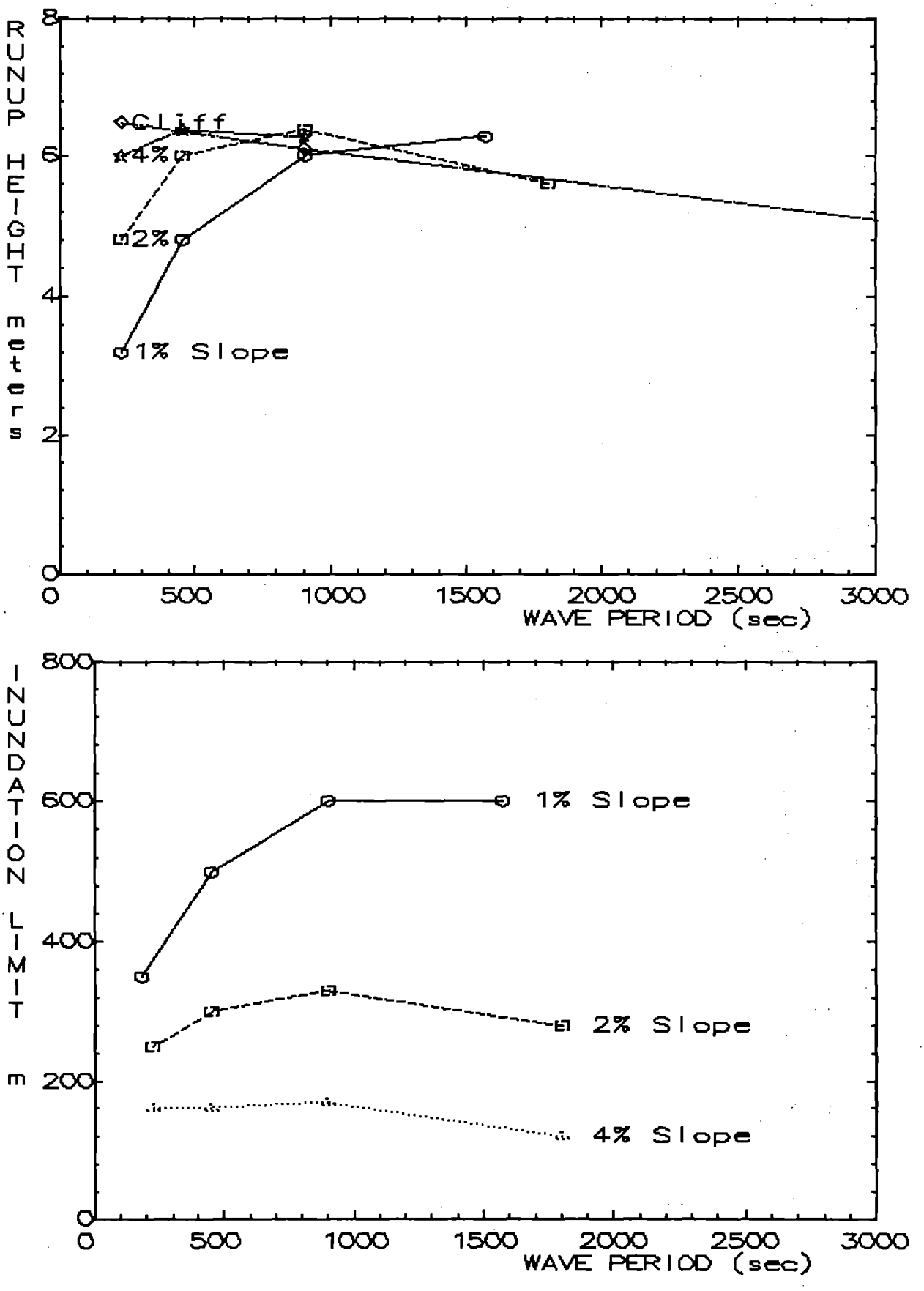

Fig. 3. Period vs flooding by a 3 m high SWAN tsunami.

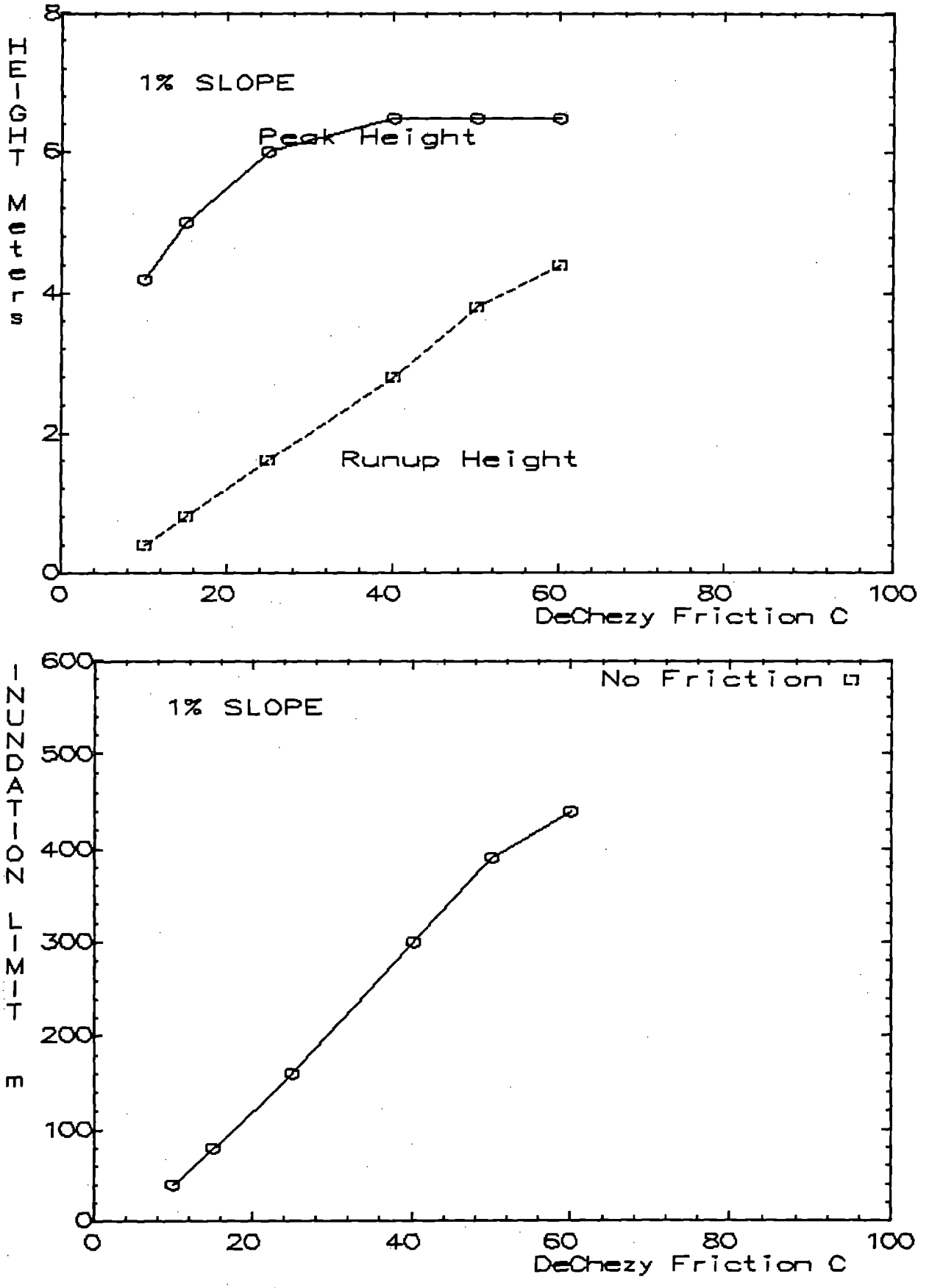

Fig. 4. Friction vs flooding by a 900 sec, 3 m high SWAN tsunami.

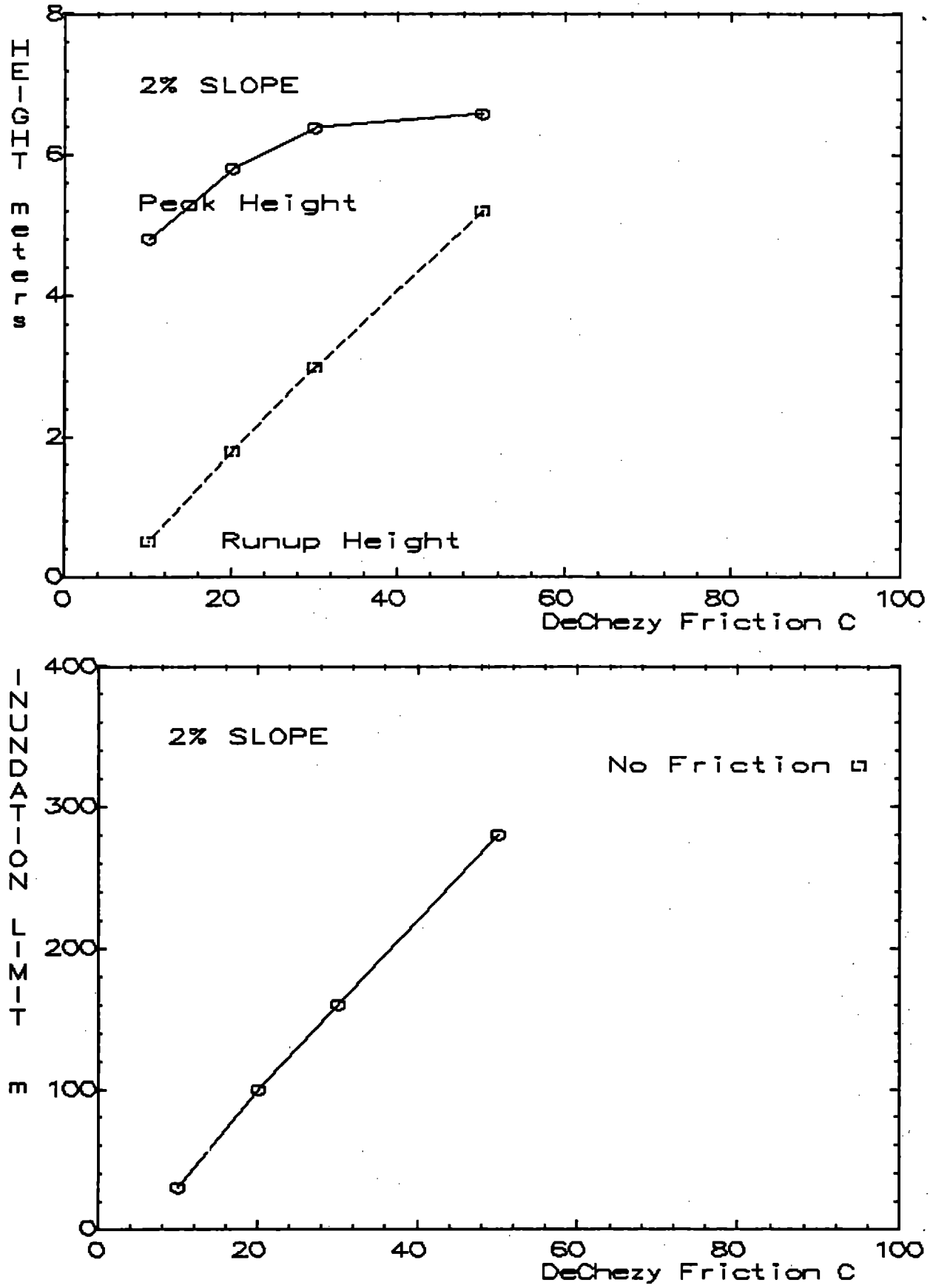

Fig. 5. Friction vs flooding by a 900 sec, 3 m high SWAN tsunami.

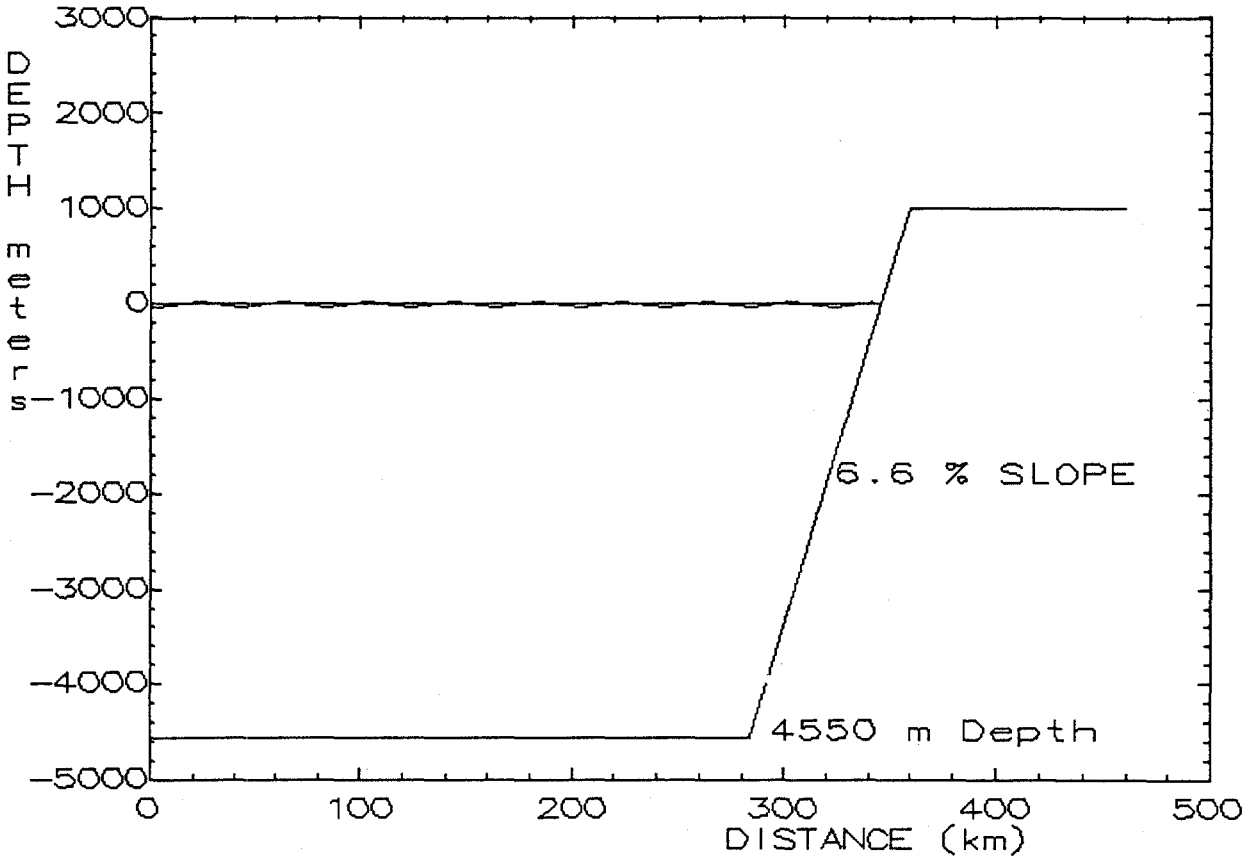

Fig. 6. Geometry for ZUNI tsunami study.

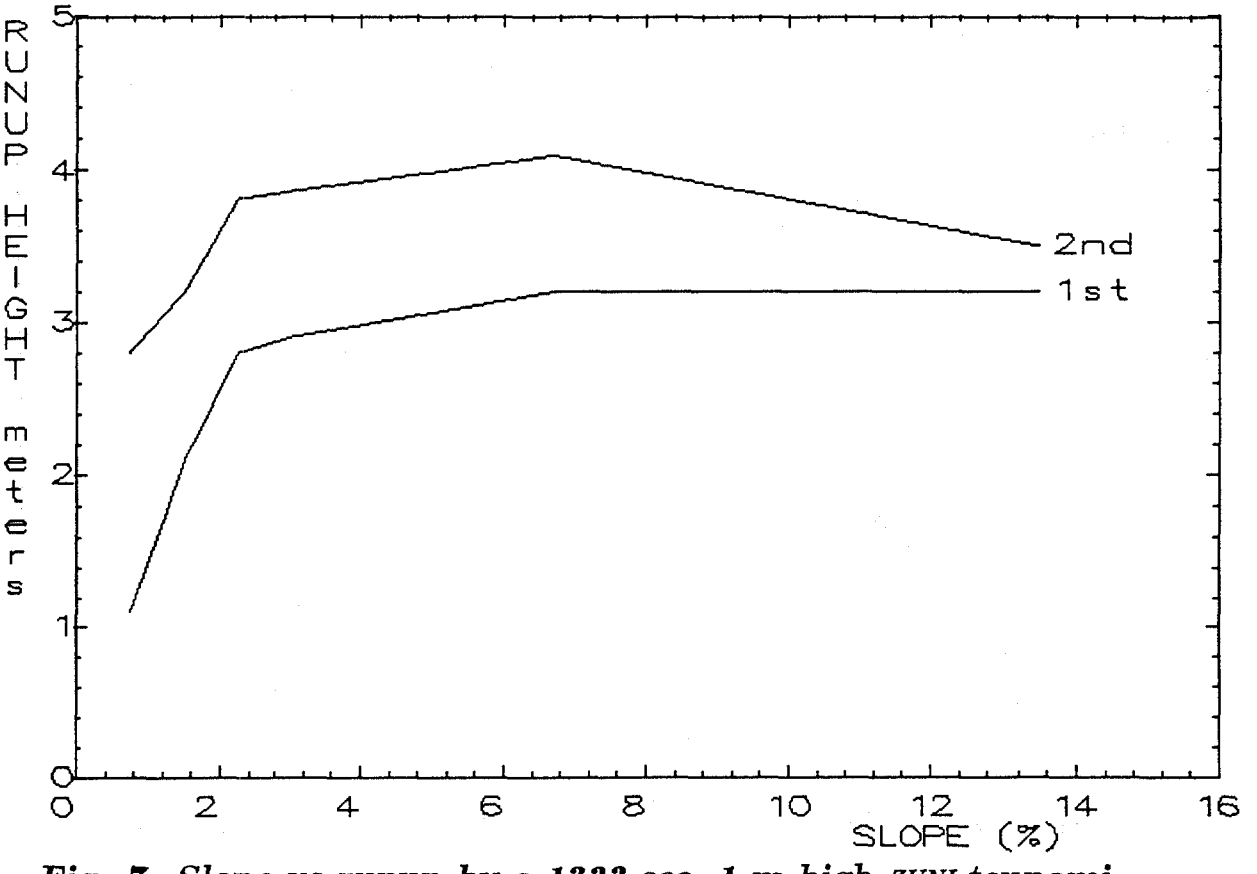

Fig. 7. Slope vs runup by a 1333 sec, 1 m high ZUNI tsunami.

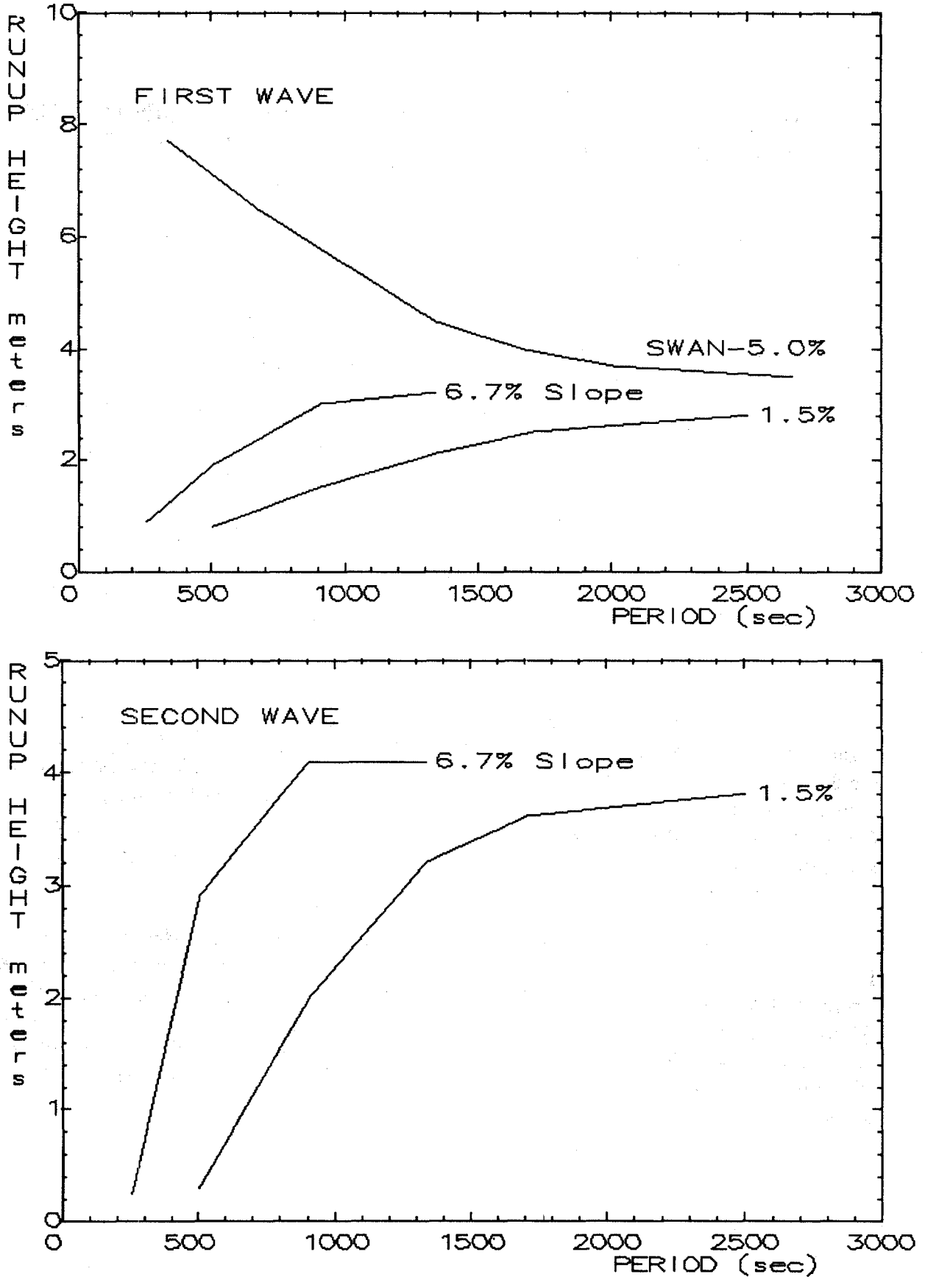

Fig. 8. Period vs runup by a 1 m ZUNI and SWAN tsunami.

NUMERICAL SIMULATION OF TSUNAMI AMPLITUDES ON THE COAST OF BRITISH COLUMBIA DUE TO LOCAL EARTHQUAKES

Max Ng*, Paul H. LeBlond*, Tad S. Murty**

*Department of Oceanography
University of British Columbia
6270 University Boulevard
Vancouver, B.C., V6T 1W5, Canada

**Institute of Ocean Sciences
Department of Fisheries and Oceans
9860 W. Saanich Road
P.O. Box 6000, Sidney, B.C., V8L 4B2, Canada

ABSTRACT

Strong evidence suggests that the Cascadia subduction zone, off the west coast of Canada and the United States, is strongly seismically-coupled and that a possible megathrust earthquake might occur in that area in the near future. A seismic sea wave, or tsunami, is a major risk associated with a megathrust earthquake. A study of tsunami hazards along the Canadian west coast due to a hypothetical earthquake is presented in this report. Numerical simulations of tsunami generation and propagation have been carried out using three models based on shallow water wave theory.

Three cases of ground motion representing the ruptures of different crustal segments in the area have been examined. Computed results provide information on tsunami arrival times and a general view of the wave height distribution. The outer coast of Vancouver Island was found to be the most strongly affected area. At the head of Alberni Inlet, wave amplitudes reached up to three times the source magnitude. Inside the Strait of Georgia, the wave heights are significant enough to receive closer attention, especially in low-lying areas.

1. INTRODUCTION

The Cascadia subduction zone off the west coast of Canada and the United States is a 1400-km-long region composed of four segments: the Winona, Explorer, Juan de Fuca and Gorda South plates (Fig. 1). Subduction takes place about 100 km seaward of Vancouver Island, where the oceanic and continental plates meet.

Two distinguishing features of the Cascadia subduction zone were reported (Heaton and Kanomori, 1984; Heaton and Hartzell, 1987; Rogers, 1988; Dragert and Rogers, 1988; Dragert and Horner, 1989). One is the absence of any historic shallow-thrust earthquakes across the plate interface since European settlements were established there about 200 years ago. Such a long-lasting seismic quiescence is shared by other subduction zones such as southern Chile, southwestern Japan and Colombia, where long periods of time elapse between violent events. Another is that the subducting segments are relatively young, ranging from 6 to 10 million years of age.

Young lithosphere such as the Cascadia subduction zone is considered to favor strong coupling because of its high buoyancy, permitting a large normal force across the plate interface, and also because of its flexibility, allowing a larger area of contact. Other physical features suggesting that the Cascadia subduction zone may be strongly coupled include the absence of active back-arc basins in the northwestern United States, the gentle dipping of the subducted slab (10° to 15°), the shallow depth of oceanic trenches, and the smooth topography of the Juan de Fuca plate. More details can be found in Heaton and Kanamori (1984).

The possibility of strong coupling between the plates implies an accumulation of elastic strain. Upon reaching the elastic limit, the strain is released and an earthquake occurs. The deduced sea-bottom displacement pattern in the British Columbia coast would include an uplift along the deformation front off the west coast of the Vancouver Island, accompanied by coastal subsidence in the northeastern and southern parts of the island (Fig. 2).

The four segmetns of the Cascadia subduction zone are of slightly different ages and might rupture independently, resulting in a sequence of several great earthquakes with magnitudes of about 8. If all segments ruptured as a whole, a giant earthquake of magnitude over 9 would result. In all cases, Dragert and Horner (1989) estimated a maximum uplift of 5 m at the rupture front and a maximum subsidence of 0.5 m in coastal regions. The form of the bottom displacement acting as the source of a potential tsunami is shown in plane view in Fig.2a, in a vertical section in Fig.2b and in perspective in Fig.2c.

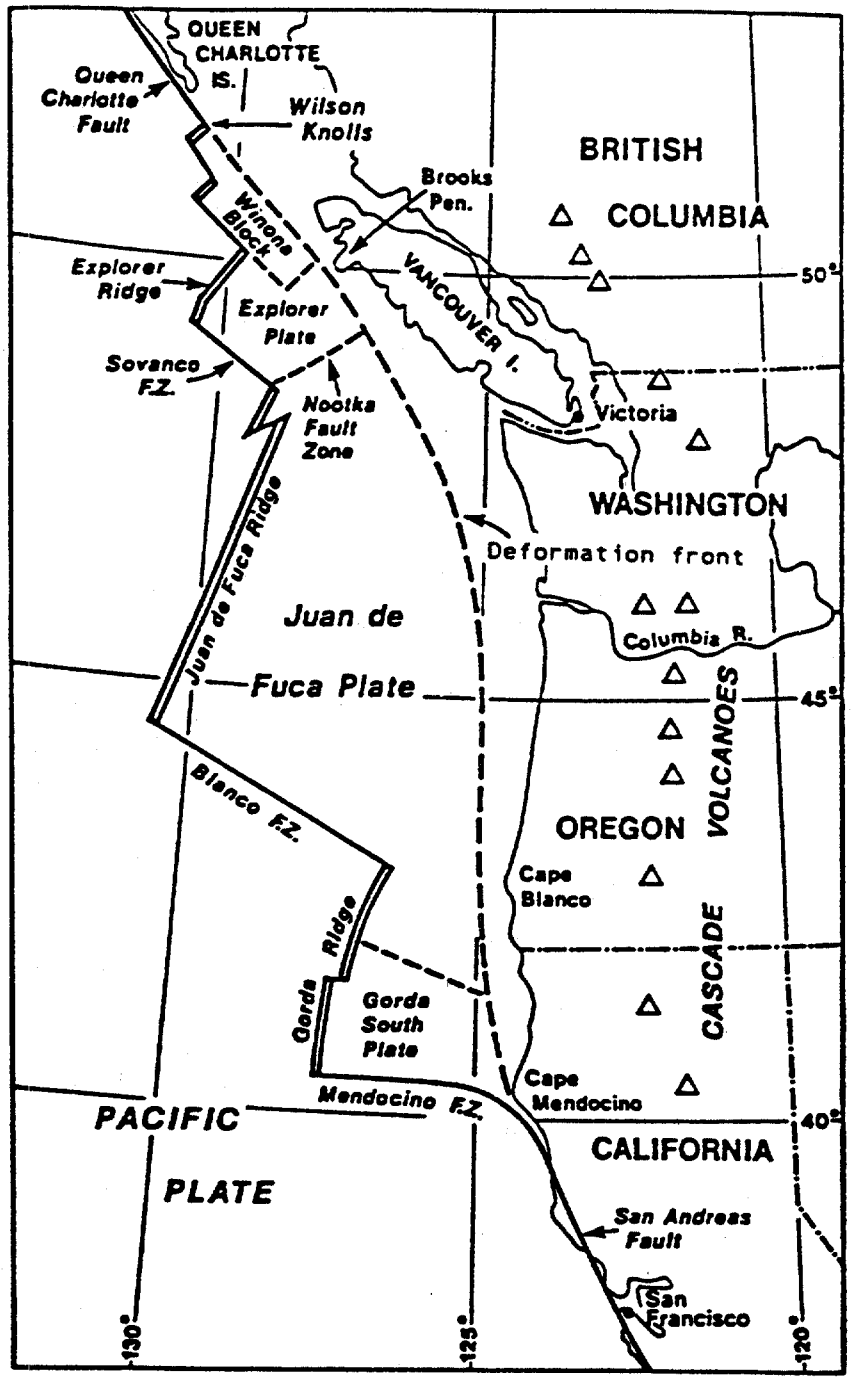

Figure 1: The Cascadia subduction zone, showing the location of four different segments. The rupture or 'deformation' front is denoted by dashed lines. (After Rogers, 1988).

2. TSUNAMI GENERATION AND PROPAGATION MODELS

To calculate the tsunami response on the British Columbia coast, three models covering different areas were developed: a two-dimensional, 5-km mesh deep-ocean model for tsunami generation and propagation across the continental shelf region; a two-dimensional fine grid model of 2-km grid spacing for wave propagation into Juan de Fuca Strait and the Strait of Georgia; and a one-dimensional inlet model, also of 2-km grid intervals, for tsunami propagation into Alberni Inlet.

(i) THE DEEP-OCEAN MODEL

A tsunami, with an amplitude small compared with both wavelength and ocean depth, is well described over relatively short propagation distances by the shallow water equations:

$$\eta_t = -(du)_x - (dv)_y \quad (1)$$

$$u_t + uu_x + uv_y = -g\eta_x + fv - ku\backslash U\backslash d \quad (2)$$

$$v_t + uv_x + vv_y = -g\eta_y - fu - ku\backslash U\backslash d \quad (3)$$

where U = (u,v), with u, v the vertically averaged horizontal velocities in the x and y directions respectively, $\eta$the elevation of water surface above mean level, d the mean water depth, f the Coriolis parameter, and k the dimensionless quadratic friction coefficient.

The forcing term in the numerical modelling of tsunami comes in the form of water surface elevation caused by the underlying sea bottom vertical displacement. In the simulated source region adopted here, the vertical sea bottom displacement is assumed to occur instantaneously and simultaneously at every depth point across the displacement zone. In other words, the time evolution of the bottom displacement is not included in the continuity equation of the ocean layer (Eq.1).

The area of study is contained in two rectangular grids (Fig.3): a coarse grid encompassing the north coast of British Columbia's mainland, the Queen Charlotte Islands and the west coast of Vancouver Island, and a fine grid encompassing Juan de Fuca Strait, the Strait of Georgia and several narrow channels and fjord systems in the mainland. The choice of rectangular cartesian grids over spherical polar grids is justified by examining the effect of the Earth's curvature on the computed wave amplitudes. By conserving energy flux within the model latitude range (45.3°N to 56.9°N), the error of neglecting the Earth's curvature is estimated to be about 6% of the computed wave amplitudes. For more details, readers are referred to Ng (1990).

The two dimensional coarse grid of resolution 5x5 km^2 is centred at 129.5°W, 51.5°N and is oriented at an angle of 30° with respect to the East (Fig.3). The numerical scheme employed in the coarse grid is the explicit one-sided difference scheme in space and time

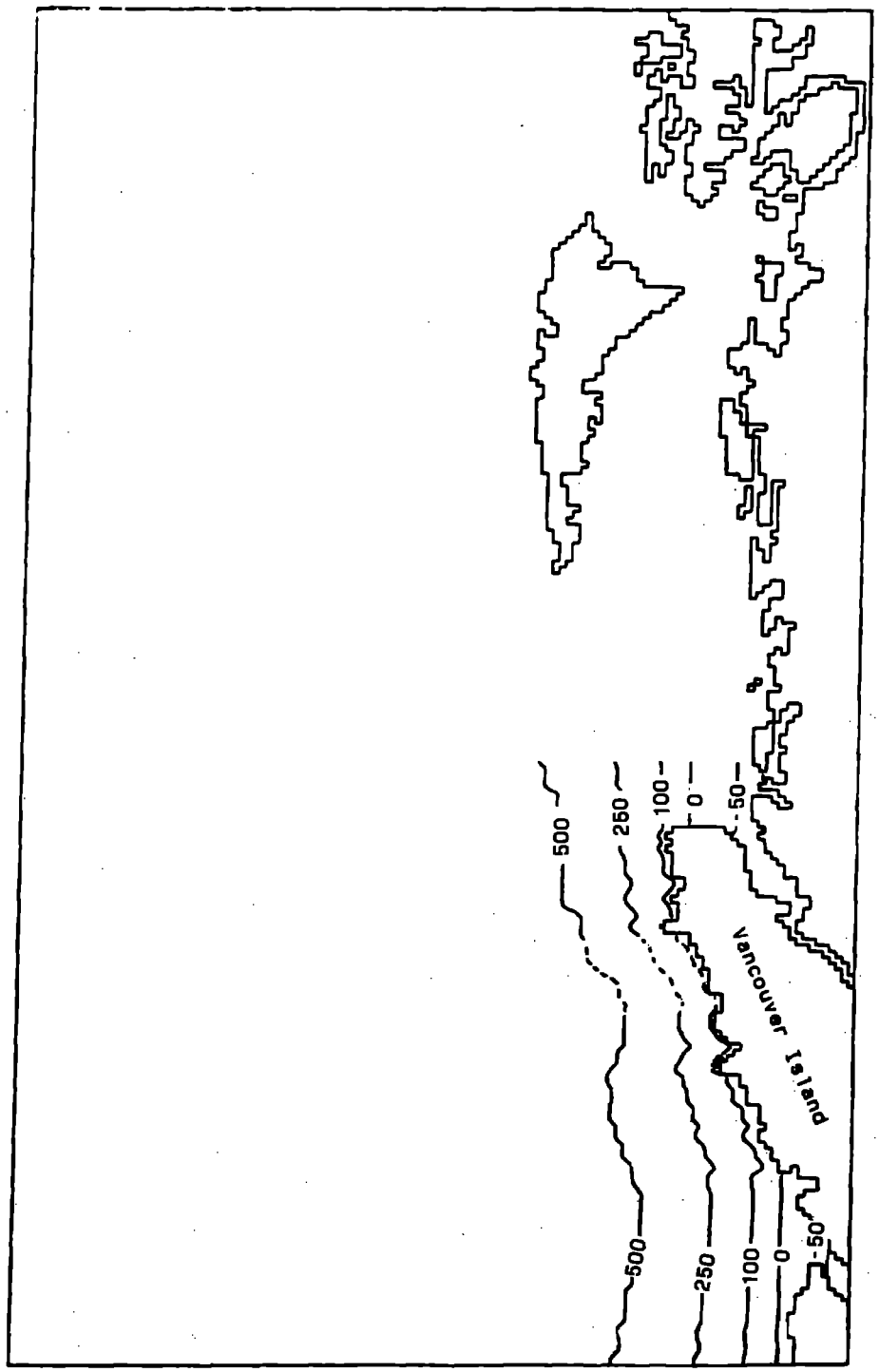

Figure 2: (a) Contours of sea-bottom displacement (in cm) with all three segments ruptured as a single unit: the Explorer segment is shown in dashed lines with the Winona segment in the north and the Juan de Fuca segment in the south. Ground motion includes a maximum uplift of 5m along the rupture front and a subsidence of about 0.5m in coastal regions.

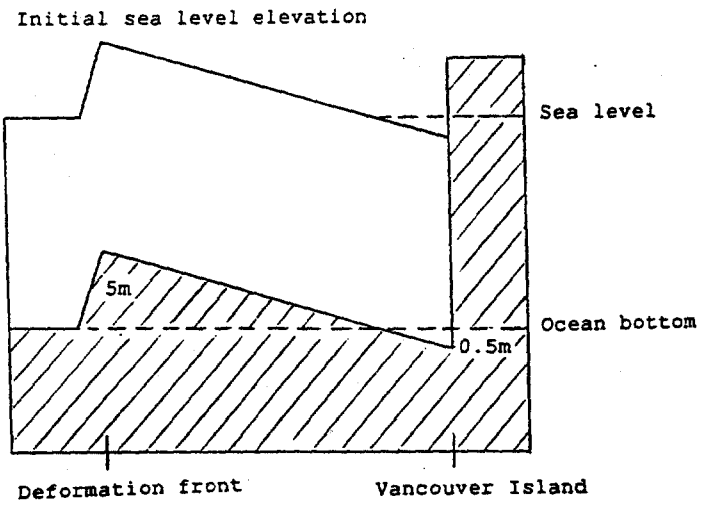

Figure 2: (b) Two dimensional cross-section view of the bottom displacement.

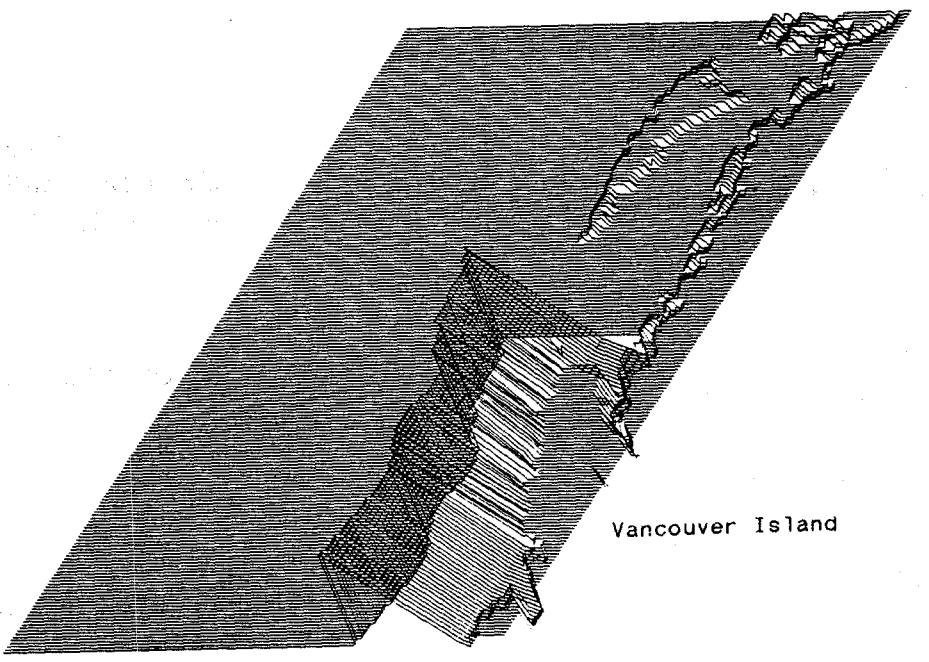

Figure 2: (c) Three-dimensional view of the bottom displacement.

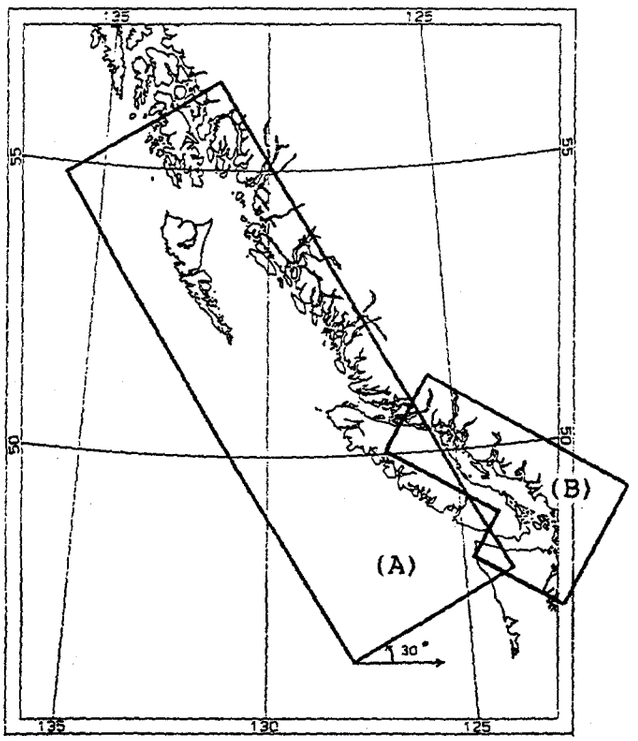

Figure 3: Location map of the study area for the west coast of British Columbia. The 5 km coarse grid (A) is used for wave propagation modelling in the ocean-continental shelf region, while the 2 km fine brid (B) is for relatively shallower waters. (After Dunbar et al., 1989).

and time using an Arakawa-C-type grid (Fig.4). The explicit nature of the scheme requires the Courant-Friedrich-Lewy condition to be satisfied:

$$\Delta t \leq \frac{\Delta x \Delta y}{[g d_{max}((\Delta x)^2 + (\Delta y)^2)]^{\frac{1}{2}}}$$

Details on the numerical solutions of Eqns.(1) to (3) can be found in Henry (1982) and Ng (1990).

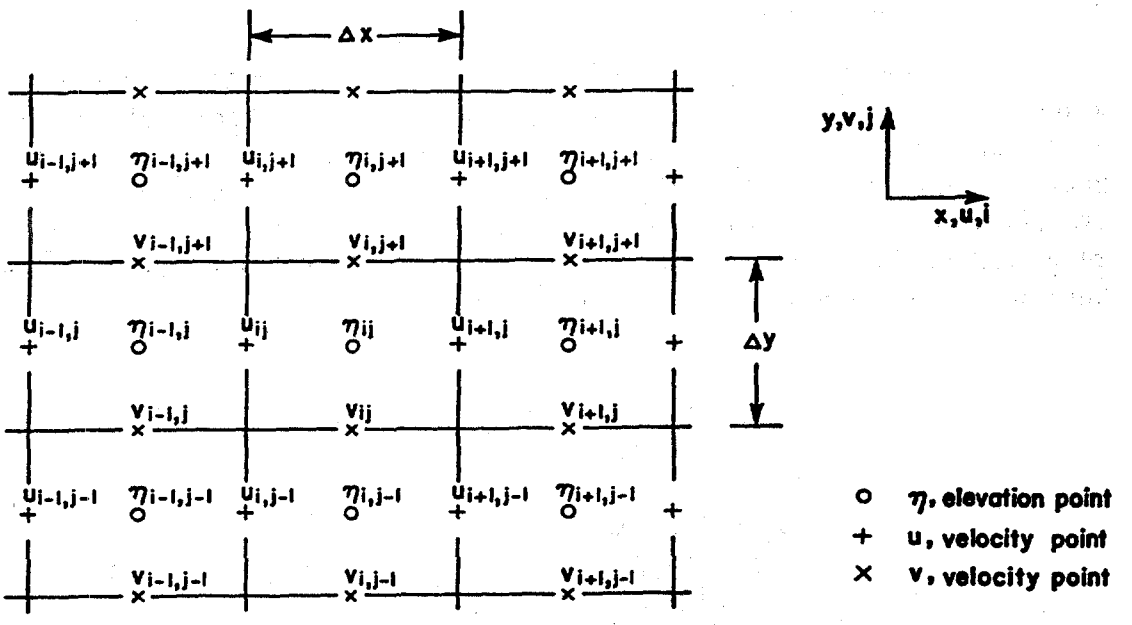

Figure 4: Arakawa-C-type grid. (After Henry, 1982).

(ii) BOUNDARY CONDITIONS

At closed boundaries, a zero velocity is assumed, and hence no volume transport is allowed. This boundary condition is equivalent to complete reflection of the wave at the coastline. At the seaward open boundaries, waves are allowed to radiate out of the model domain from the interior by applying the radiation condition. The velocity vector are treated one-dimensionally on the boundary, and the radiation boundary condition reads

$$u(\text{or } v) = \pm\sqrt{\frac{g}{d}}\,\eta, \tag{4}$$

where the ± sign depends on the direction of propagation. Spurious reflections from the artificial open boundary are further reduced by augmenting the coarse grid with a constant-depth westward extension.

(iii) MODEL VARIABILITY

The deep-ocean model applied on the coarse grid, as mentioned above, is adopted from Henry (1982), who applied it successfully to the Beaufort Sea. The model has also been used in previous tsunami applications, for example, by Murty and El-Sabh (1985) in the St. Lawrence estuary, and by Crean et al (1988) in modelling the 1946 earthquake near Comox, Vancouver Island.

(iv) THE FINE GRID MODEL

After the tsunami propagates into Juan de Fuca Strait, it goes through a complex series of narrow islands and channel divisions at the southern and northern entrances of the Strait of Georgia, where damping and nonlinear interactions might result. A relatively finer grid model than the deep-ocean model is obviously necessary to account for the irregularities of the topography and coastline configuration. A 2-km mesh vertically-integrated model adapted directly from the GF7 model of Crean et al (1988) serves this purpose. The model layout is shown in Fig.5.

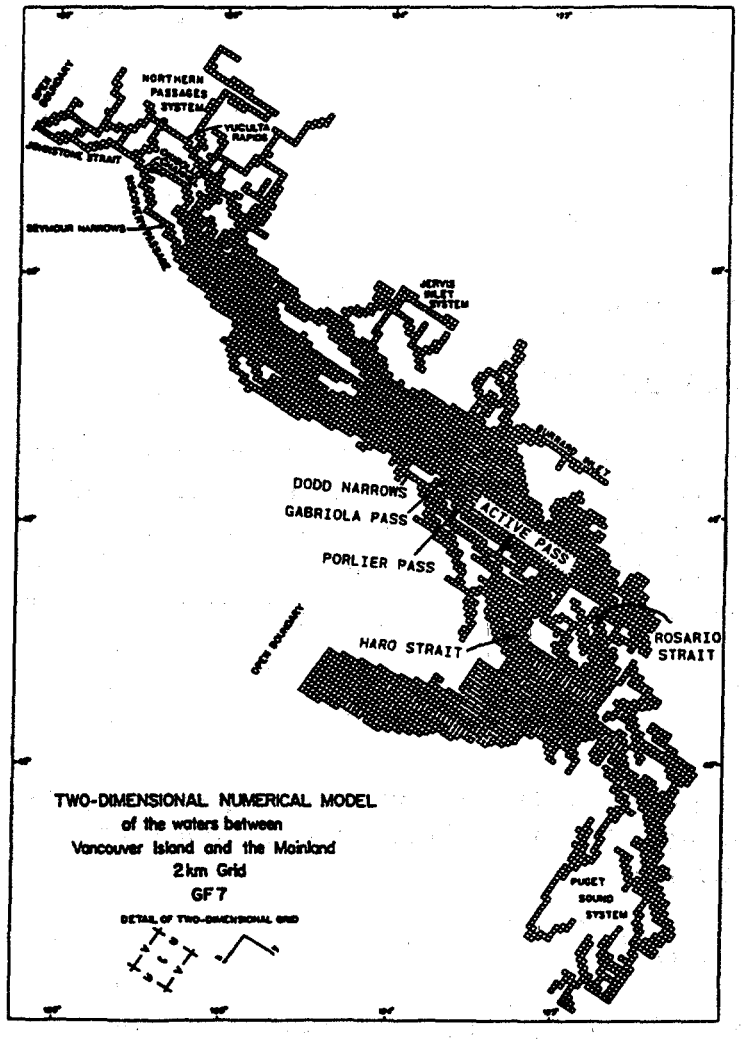

Figure 5: Geographical location of the fine grid model. (After Crean et al., 1988).

The fine grid model is basically similar to the deep-ocean model, but some differences do exist. The vertically-integrated equations of continuity and momentum are

$$\frac{\partial \eta}{\partial t} + \frac{\partial q_1}{\partial x} + \frac{\partial q_2}{\partial y} = 0 \tag{5}$$

$$\frac{\partial q_1}{\partial t} + \frac{\partial}{\partial x}\left[\frac{q_1^2}{d+\eta}\right] + \frac{\partial}{\partial y}\left[\frac{q_1 q_2}{d+\eta}\right] - fq_2 + g(d+\eta)\frac{\partial \eta}{\partial x} + \frac{kq_1|q|}{(d+\eta)^2} = 0 \tag{6}$$

$$\frac{\partial q_2}{\partial t} + \frac{\partial}{\partial x}\left[\frac{q_1 q_2}{d+\eta}\right] + \frac{\partial}{\partial y}\left[\frac{q_2^2}{d+\eta}\right] + fq_1 + g(d+\eta)\frac{\partial \eta}{\partial x} + \frac{kq_2|q|}{(d+\eta)^2} = 0 \tag{7}$$

where $q_1 = u(d + \eta)$, $q_2 = v(d + \eta)$, with u,v the vertically averaged velocities as defined in the deep-ocean model. The previous assumption of $(d + \eta) = d$ in the deep-ocean model does not apply here because the magnitudes of η and d may become comparable in shallow waters. This difference results in additional nonlinear terms, such as, in the momentum equations: $g\eta\eta_x$ and $g\eta\eta_y$. Similar changes occur on the friction terms. The numerical scheme employed here is again similar to that in the deep-ocean model: explicit one-sided differencing in space and time. The finite-difference forms of Eqns. (5) to (7) can be found in Crean et al. (1988).

Another major change from the deep-ocean model is the variability of bottom friction coefficients. Since friction effects and their local variation are more important in shallow depths, a regional distribution of dissipation was allowed by varying coefficients of bottom friction. As discussed in Crean et al. (1988), by fitting the computed amplitudes of the M_2 tidal constituent to the measured values, the overall frinction coefficient was set to 0.003, with the following exceptions: the Puget Sound system and Rosario Strait (0.006); Haro Strait (0.03); Active, Porlier, Gabriola Passes, and Dodd Narrows in the southern Gulf Islands (0.03); Seymour Narrows (0.006), Okisollo Channel (0.03), and Yuculta Rapids (0.03) of the northern passages. Locations of the channels and passes are shown in Fig.5.

(v) BOUNDARY CONDITIONS

Coastal boundaries are characterized, as usual, by zero normal components of velocity vectors. Open boundaries are taken along the junctions between the coarse and fine grids where prescribed elevations are obtained from the deep-ocean model.

Matching conditions between the two grids were examined to determine the find grid model's sensitivity to the junction values. Several configurations of open boundaries on the coarse grid, for instance, were tested. On the other hand, spurious reflections from the boundaries are reduced by allowing a large overlap area. The spatial arrangement of the fine and coarse grids at the Juan de Fuca Strait junction is shown in Fig.6. Prescribed elevation boundary values on the fine grid model are obtained directly from the deep-ocean model and are interpolated spatially and temporally before application. A four-point linear interpolation scheme is used to estimate the fine grid boundary elevation points, as is illustrated in Fig.7. At the northern passage, the junction consists of only one grid point and is set to the nearest elevation point available in the coarse grid. No spatial averaging is necessary.

It is further assumed that the deep-ocean and fine grid models are coupled independently; that is, the deep-ocean model is operated as if the waves reflected from the fine grid domain did not enter the coarse grid region. This assumption is adequate if the tsunami is significantly absorbed, rather than reflected, within the Strait of Georgia-Puget Sound system.

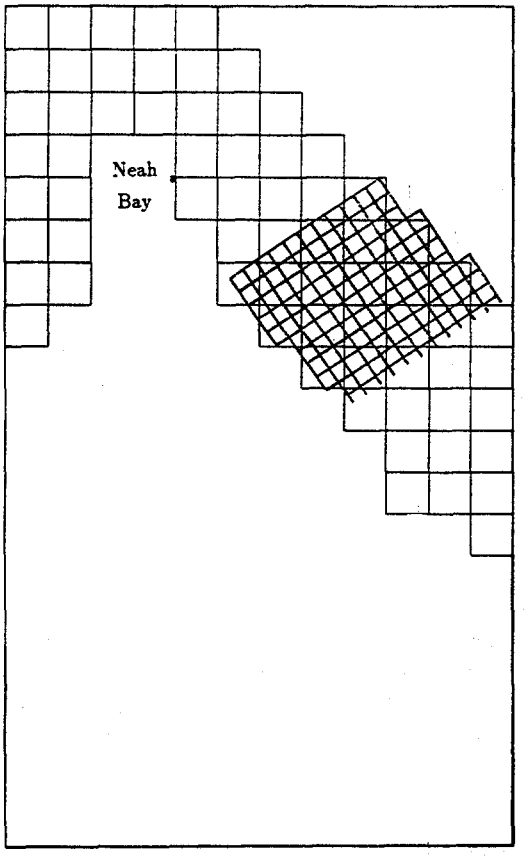

Figure 6: Junction of the fine grid and extended coarse grid at the Juan de Fuca Strait.

(vi) TSUNAMI PROPAGATION IN INLETS

Wave magnification in coastal waters arises from a number of factors, such as reflection, refraction, funnelling and resonance. Relatively large wave amplitudes may result if some of these factors come into effect together. An example in the west coast of Canada is given by Port Alberni on Vancouver Island. The City of Port Alberni which is located at the head of Alberni Inlet has experienced a number of tsunamis in historic times. Of particular interest is a 4 m tsunami triggered by a distant source during the 1964 Alaskan earthquake. The large-amplitude waves observed at Port Alberni are due to the combined effects of the topographic amplification in Barkley Sound and the resonance magnification in the inlet (Marshall Macklin Monaghan, 1986; Murty and Boilard, 1970). Because of Port Alberni's high risk to tsunami threats, Alberni Inlet is chosen for some detailed study.

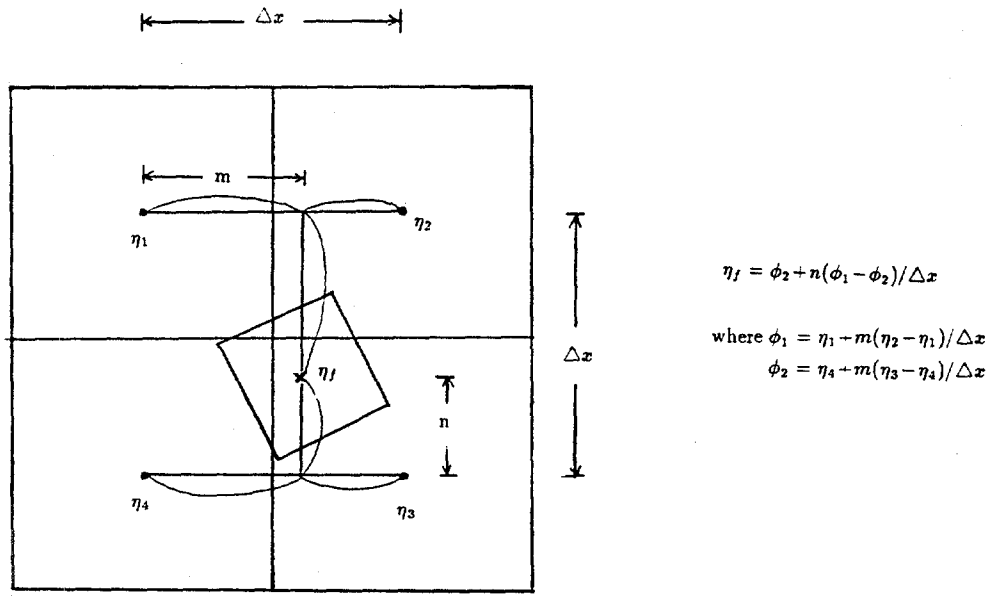

Figure 7: Four-point interpolation scheme used in calculating the fine grid open boundary values.

Fig. 8 shows the location of the City of Port Alberni. For simplicity, the inlet is represented as a one-dimensional system. This representation is justified on the grounds that the width of the inlet is much smaller than its length. Branchings of channels are neglected in the study. It is further assumed that the inlet model is operated independently from the deep-ocean model.

(vii) THE INLET MODEL

The inlet model is based on the one-dimensional, depth averaged equations of continuity and momentum

$$W\eta_t + Q_x = 0 \tag{8}$$

$$\left(\frac{Q}{A}\right)_t + g\eta_x + \frac{\tau_h}{\rho d} = 0 \tag{9}$$

where Q is the transport (m^3/s) given by $Q = uWd$, with u the vertically averaged velocity as defined in the deep-ocean model, W the surface width of the inlet, d the water depth, A the cross sectional area of the inlet, τ_h the frictional shear stress, and ρ the density of water. Because of the importance of friction dissipation in shallow waters, friction

coefficients are allowed to vary at each grid point. Equations (8) and (9) have been applied by several authors in previous studies of tsunami response in inlets, as referenced in Dunbar et al. (1989). The numerical solutions are obtained using an explicit, one-sided differencing scheme, as in the previous two models. Details can be found in Dunbar et al. (1989) and Ng (1990).

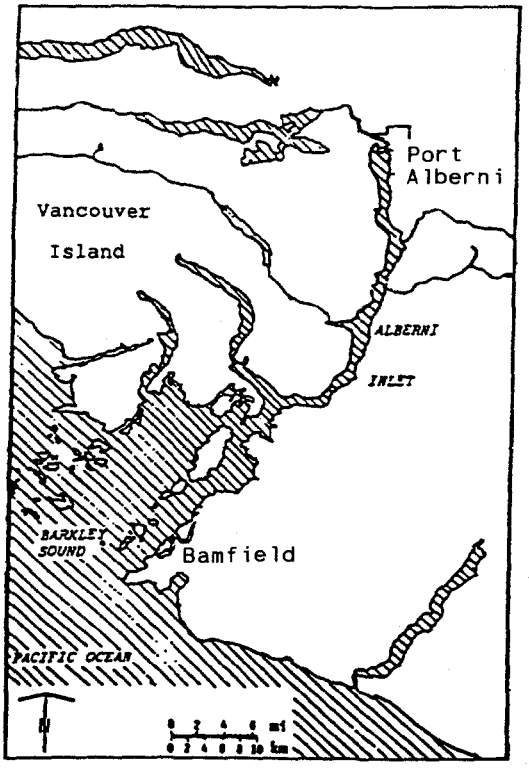

Figure 8: The geographical location of Alberni Inlet. (After Marshal, 1986).

(viii) BOUNDARY CONDITIONS

(a). Closed boundaries

As in the previous cases, a condition of zero normal velocity is imposed at the closed boundary. This complete-reflection assumption is, however, true only for steep coasts. On gently sloping beaches, as is our case, the wave runs inland and dissipates much of its energy through inundation of the surrounding land. As pointed out repeatedly by Dunbar et al. (1989), the zero-velocity boundary condition would over-estimate the computed water-levels

at the inlet head by neglecting the wave dissipation from flooding. The accuracy of modelling wave response at the inlet head could be improved by taking into account the run-up process, including possible bore formation and rushup, through use of fine resolution models with more realistic boundary condtions, for instance, the moving water line condition.

(b). Open boundaries

Prescribed open boundary values at the mouth of the inlet are provided by the deep-ocean model at Barkley Sound. The stored coarse grid data are linearly interpolated before application. It is noted that because of the narrow width of the inlet compared to the wavelength, not all wave energy at Barkley Sound would propagate up the inlet. As a result, modelled wave amplitudes along the inlet could be improved by separating the wave at Barkley Sound into incoming and reflected outgoing components. These improvements are left to further studies.

3. RESULTS

Three cases of sea-bottom displacement in the Cascadia subduction zone were studied for the tsunami generation and propagation problem: the rupture of, first, the three upper segments all at once; second, of only the largest segment, the Juan de Fuca segment; and, third, of both the Winona and Explorer segments but not of the Juan de Fuca segment.

A rupture of all three segments would represent the worst scenario studied here, which is equivalent to an event of seismic moment magnitude (Mw) of over 9.2 (Rogers, 1988). This was, however, reported to be unlikely as different subducting segments are of slightly different ages and may rupture independently. If the rupture is confined to the Juan de Fuca segment, it would cause a magnitude 9.1 earthquake. If the Winona and Explorer segments rupture together, a magnitude 8.7 event would result. Al three cases include regions of uplift and subsidence, the first case of which is shown in Fig.2, with a maximum elevation of 5 m along the deformation front and a maximum 0.5 m submergence along the northeast and southwest coast of Vancouver Island. The length of the deformation front is about 500 km for the first case, 290 km for the second and 210 km for the third.

Numerical simulations using the three models discussed in the previous chapter were performed for the associated tsunami problem, and results are presented in the forms of a first-wave travel time chart to give an overall view of the propagation of the tsunami wavefronts and plots of wave amplitude time-series at various coastal locations to illustrate the local tsunami response. The selected regions include some major tide-gauge locations and populated areas along the western British Columbia coast. Finally, three-dimensional snapshots of sea surface displacement in the deep-ocean model region are given at selected time intervals to provide another view of the propagating wavefronts.

(i) RUPTURE OF THE JUAN DE FUCA, WINONA AND EXPLORER SEGMENTS

The tsunami leading-wave travel time chart is shown in Fig.9 for the first case of bottom displacement. Refraction occurs as waves approach the shores. Time-series plots of simulated tsunami waves are given in Figs. 11, 12, 14 and 15. Several stations, with their locations shown on Fig.10, are chosen here for discussion.

Fig.11 shows the sea-level variation at a point located above the rupture front. The elevation of water level is seen to drop rapidly from the initial 5 m uplift as the

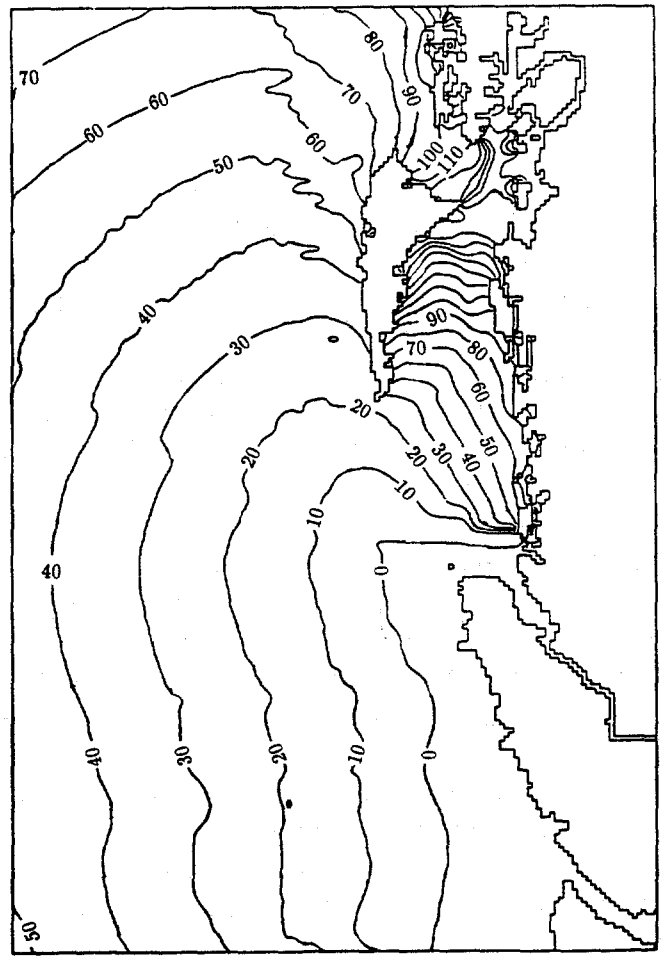

Figure 9: Tsunami travel times (in minutes) in the deep-ocean model domain for the case in which all three segments rupture together. Contour intervals are 10 minutes.

wave energy propagates away, and the sea surface appears to be relatively calm after twelve hours, confirming the lack of reflection from the seaward edge of the numerical model. The rupture front is located around the 2,000 m bathymetric line, and the wave response discussed here displays some common features usually observed at other deep-ocean points in the model: a broad spectrum, without resonances and with small amplitudes.

Fig.12 shows the time series of sea level displacements at Cape St. James, whose high frequency appearance is very similar to Fig.11. Cape St. James, situated at the southern tip of the Queen Charlotte Island, is explosed directly to the open sea and has a narrow continental shelf that keeps wave shoaling to a minimum. Amplification of the wave through resonance does not take place. The response at Cape St. James is therefore very similar to that of the open ocean.

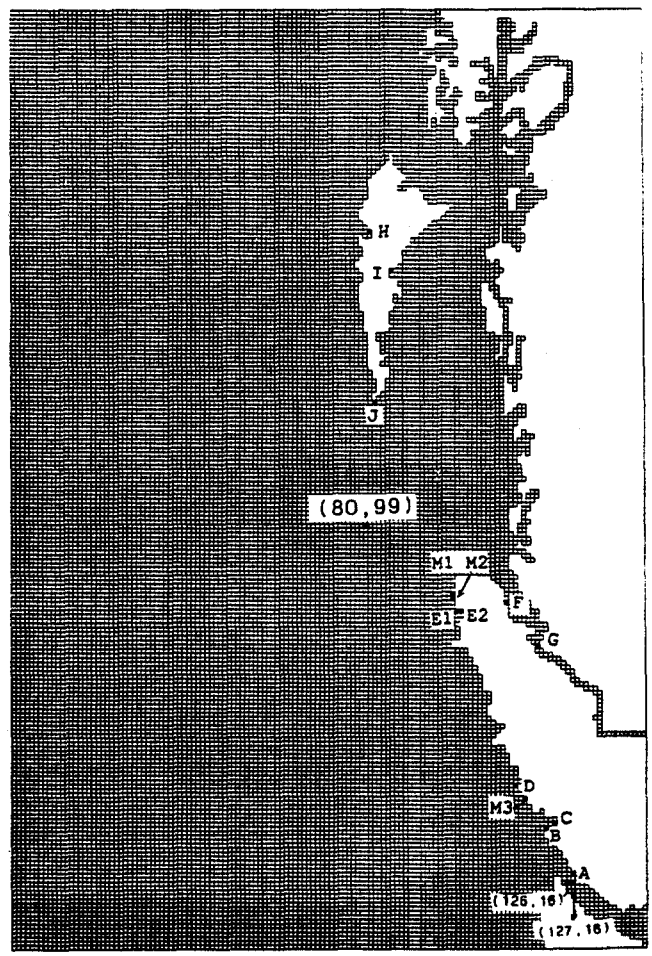

Figure 10: The coarse grid layout showing the locations at which time histories of water level are plotted.

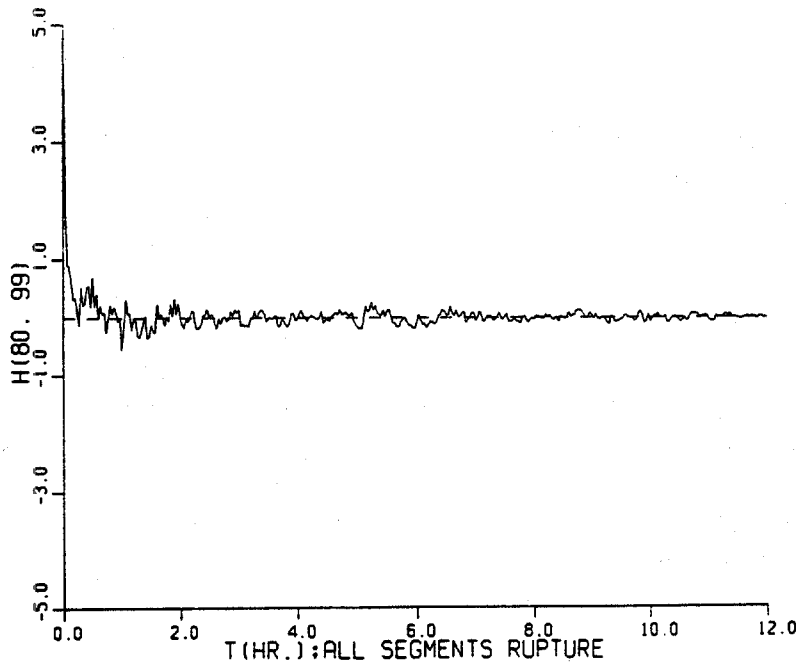

Figure 11: Computed elevation (in m) of one of the source points located above the deformation front for the case of all three segments ruptured together. The initial elevation is 5.0 m. Station location is shown in Fig. 10.

In Rennel Sound and Queen Charlotte City (Fig.12 H & I), both located north of Cape St. James, relatively large wave amplitudes are observed when the waves reach the shallow shorelines. This amplitude build-up is commonly observed in coastal regions where the continental shelf is wide enough to cause wave shoaling. Shoaling results from a decrease of water depth and a slow down in wave velocity which, when conserving energy flux, would imply an increase of wave amplitudes. On the other hand, waves may also be amplified by refraction. As stated earlier, refraction bends the wave when approaching the shore. The wave number vector continuously changes direction so as to approach the shore normally and so does the energy flow vector. Energy can therefore be focussed. These two effects may explain responses of some other locations along the western Vancouver Island, for instance, Bamfield and Tofino (Fig.12 B,D).

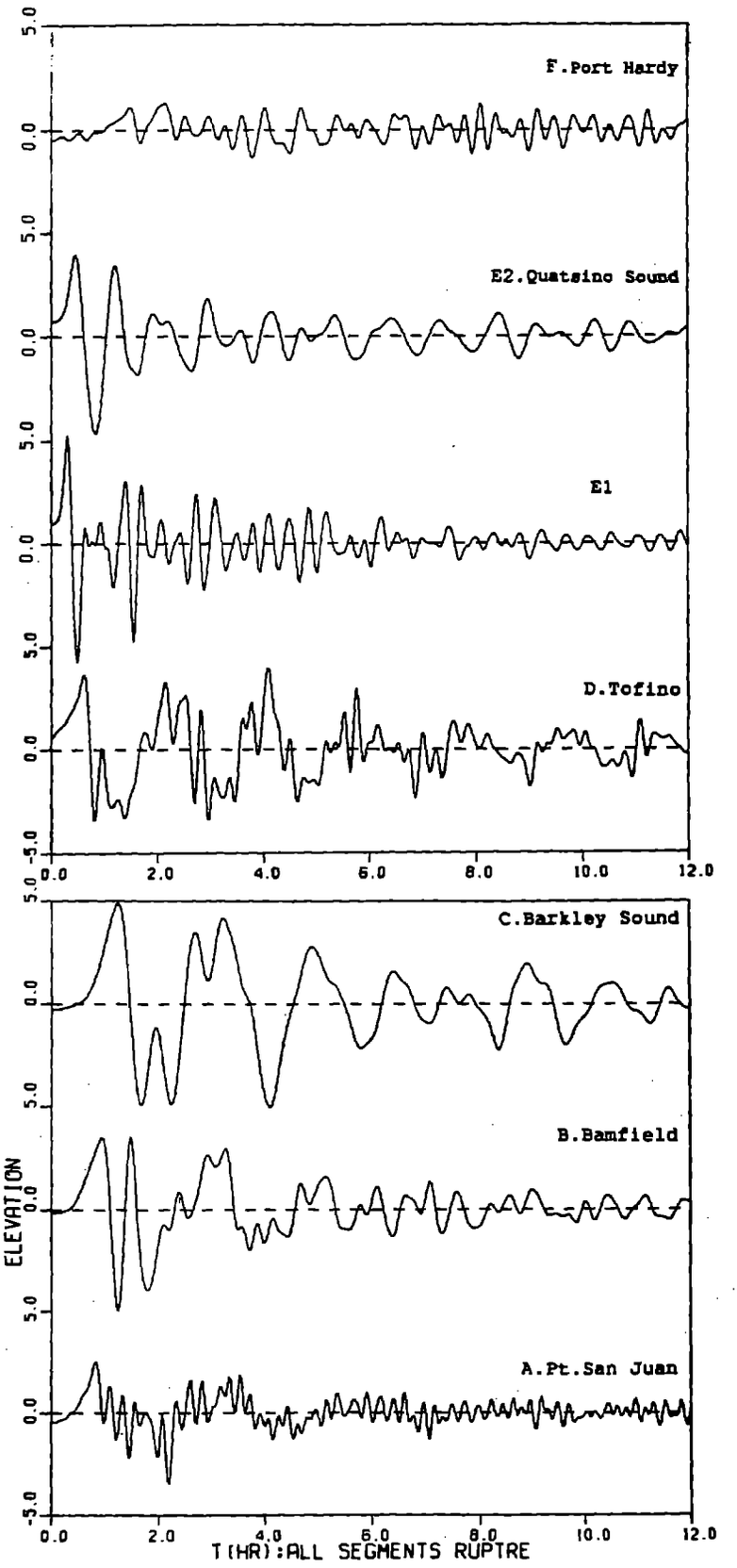

Figure 12: Time-series of computed elevation in the deep-ocean model for the case of all three segments ruptured together. Station locations are indicated in Figure 10. the vertical scale is given in metres.

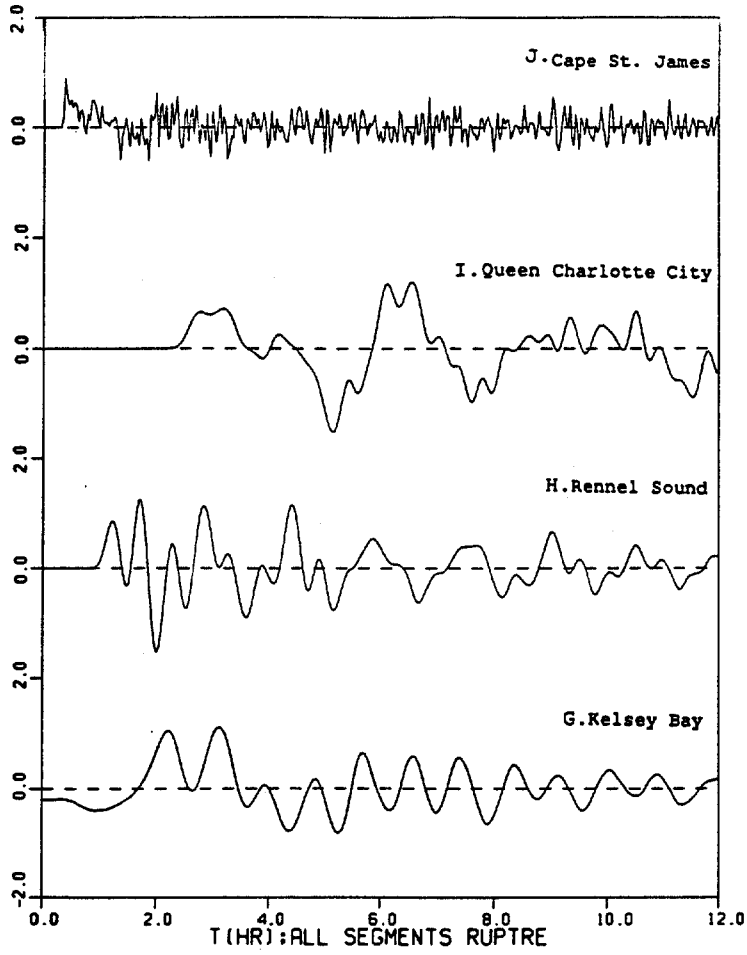

Figure 12: Continued.

In addition to shoaling and refraction, wave amplitudes at Barkley Sound and Quatsino Sound (Fig.12 C,E) appear to be further enchanced by resonant oscillations. By comparing Fig.12 E1 and E2, it is evident that certain frequencies are preferentially excited after the tsunami enters Quatsino Sound. An eigenmode of about 60 minutes seems to be present in both Barkley Sound and Quatsino Sound.

Port San Juan which is located at the northwest entrance of the Strait of Juan de Fuca shows well tuned oscillations of relatively high frequency (Fig.12A). Seiche excitation in Port San Juan has been studied by Lemon et al. (1979), who reported a fundamental resonant period of 15 minutes. This is the period which is prominent in Fig.12A.

After the tsunami propagates into the Strait of Georgia (Fig. 13), the wave amplitude is greatly attenuated partly because the wave energy continues to be dispersed over a greater area along the path of propagation and, additionally, because energy is lost to friction which becomes important in shallow waters, notably in the complex Gulf Island system. Such a

decrease in amplitude is seen in the sequence of time-series from Victoria (Fig.14) to Vancouver (Figs.13,14) where the wave is attenuated by a factor of two. The tsunami action near Vancouver, though small, is still noticeable, with an amplitude of about 60 cm. As the oscillations continue for many hours, a tsunami would be superimposed upon a high-tide and might pose some danger to low-lying areas of the Fraser River delta.

In general, elevations in the Strait of Georgia are below a metre. A growing, well tuned oscillation in the inner basin of Burrard Inlet deserves further consideration (Fig.14.16). Vancouver harbour, which behaves like a Helmholtz resonator, is seen to have a resonant period of approximately 3 hours. Following the work of Baines (1958) on a tidal model in Burrard Inlet, a resonant period of 4.1 hours was obtained. Considering the dependence of the resonant period on the exact geometry and frictional values used, this resonant period is in fairly good agreement with the one observed here.

The propagation of the tsunami into Alberni Inlet is determined by applying the inlet model, with results shown in Fig.15. The wave height at the head of the inlet is seen to be amplified about three times above that at the mouth of Barkley Sound. By comparing the maximum wave heights at the head of Alberni Inlet and Tofino (Fig.12), the ratio is approximately 4 to 1. The same ratio for the 1960 Chilean earthquake was reported by by Marshall Macklin Monaghan (1986) to be 3.2. The resonance characteristics of the inlet were also studied by Murty and Boilard (1970) with the inlet represented as a quarter-wave oscillator. The reported fundamental mode of about 85 minutes is consistent with the one computed here.

It is noted that the wave height at the inlet head might be over-estimated for the following reasons: (i) the total-reflection boundary condition at the coast does not allow the dissipation of wave energy through running up the beach; (ii) the wave energy at Barkley Sound, where it was taken to drive the inlet model, was assumed to propagate into the inlet without reflection. Reflection back to sea would remove some of the energy.

(ii) RUPTURE OF THE JUAN DE FUCA SEGMENT ALONE

In the second numerical experiment, only the Juan de Fuca segment is ruptured (Fig.16). The forcing terms at the southern half of the Vancouver Island are therefore identical to the first case, resulting in wave responses (Fig.17) that are very similar to those seen in Fig.12. The stations in the north, on the other hand, experience a drop in amplitudes due to the large spatial attenuation of wave energy (Fig.17 and Fig.12). Particularly in Rennel Sound and Queen Charlotte City (Fig.17), the waves are seen to be almost twice as small as earlier (Fig.12). Because of the similar wave signatures in the south compared to the first case of the source displacement, calculations in the Strait of Georgia - Puget Sound system and the Alberni Inlet are not repeated in this run.

(iii) RUPTURE OF THE WINONA AND EXPLORER SEGMENTS

In the third calculation, only the Winona and Explorer segments are assumed to rupture together. The forcing terms are then located in the Vancouver Island's northern half, and hence the wave characteristics there (Fig.18) look similar to Fig.12. In the southern half, the waves arrive at a later time and, as expected, are smaller in amplitude (Fig.18 and Fig.12). The Strait of Georgia system and the Alberni Inlet follow the same trend: a later arrival of waves with smaller amplitudes; the patterns of the waves are, however, preserved in general (Figs.19,20). Comparing the results on the outer coasts for the three cases of bottom displacements, it is observed that the near-field tsunami response is due mainly to nearby segments.

In Fig.21, three-dimensional snapshots of sea-surface displacements in the deep-ocean model domain are shown at selected time intervals for this particular source rupture. These pictures complement the travel time curve of Fig.9 and give another view of the propagating wavefronts. The large amplitudes are seen to concentrate along the coast of Vancouver Island, as described in the local time series (Fig.18); the seaward propagation is now evident.

(iv) MODEL LINEARITY

Because of the long wave nature of tsunamis, the nonlinear advective terms in the momentum equations are expected not to be locally important. Calculations show that nonlinearity plays a small role in computing sea-level displacements. Results obtained from the above equations and their linearized forms are almost indistinguishable. We have also found that a doubling of the source strength also results very nearly in a doubling of the tsunami response.

4. CONCLUSION

The similarity of the Cascadia subduction zone's tectonic features to those of other subduction areas in the world, together with results from recent geodetic surveys of the ground motion as well as records of prehistoric large earthquakes in the area, suggest that a megathrust earthquake may occur in western British Columbia in the near future. The compelling evidence for a large seismic event off British Columbia has prompted the study of the local tsunami response. Three numerical hydrodynamical models covering different areas of the studied region were used to calculate tsunami generation and propagation. Computed results include tsunami travel times and sea surface displacements and may provide useful information for the emergency planning response to tsunami hazards.

Three cases of source motion were studied. Simulated wave amplitudes have been plotted for major tide gauge locations and some densely populated areas along the British Columbia coast. The wave pattern observed at each location depends strongly on local topography, such as the width of the continental shelf, and the shoreline configuration, both

of which affect wave refraction and reflection, the amount of shoaling and the excitation of resonance.

Results have shown that the most affected area was along the outer coast of Vancouver Island because of its proximity to the source. Particularly at the head of Alberni Inlet, the waves are seen to be drastically magnified through resonance, with magnitudes about three times those in Barkley Sound.

The travel times of the first positive wave to Victoria and Vancouver, the two main business and commercial centres in British Columbia, are 94 and 187 minutes respectively if all three segments break as a whole and are correspondingly 127 and 226 minutes if only the Winona and Explorer segments rupture together. With the exception of those locations that are very near the source, the largest waves usually come after the leading waves, as is seen in the Strait of Georgia system. The wave amplitudes observed there, although the area is sheltered by Vancouver Island and the wave is attenuated by friction, are still significant. Around the Vancouver area, the maximum wave amplitude is approximately 1 m. Low-lying areas such as Richmond are therefore subject to threats of flooding when the tsunami arrives at high tide.

The major limitation of the tsunami amplitude computations comes from the uncertainty in specifying the source. A more confident description of source parameters such as the dimension of the displacement zone would enhance the accuracy of the computed results. The wave models, on the other hand, could also be improved in a number of ways:

1. The area of computation should be extended southwards to include the entire Cascadia zone. The Gorda plate and the lower portion of the Juan de Fuca plate were not considered in this study, which might result in different wave forms if any of these two segments were to rupture.

2. The present model has omitted a detailed study of most of the inlet systems along the British Columbia coast. Only Alberni Inlet was treated in detail in the inlet computation. The results from the deep-ocean model therefore represent only the wave response adjacent to the mouths of the inlets. Finer resolution models are required to improve the results' accuracy in bays and inlets.

3. The treatment of Alberni Inlet under the present scheme is; however, not yet complete. The results only provide the wave amplitudes at the shoreline; it does not give the run-up heights. The latter information is considered to be more important because flooding by tsunami waves causes most of the damage. The modelling of the run-up process, which may include bore formation, breaking and rushing-up, requires modification of the present assumption of zero mass transport at the coastline and development of high-resolution models to account for complex

REFERENCES

1. BAINES, W.D., 1958. Tidal currents in constricted inlets. Proc. 1958 Coastal Engineering Conference, Miami, 545-561.

2. CREAN, P.B., MURTY, T., STONACH, J., 1988. Mathematical modelling of Tides and Estuarine Circulation, Lectures notes on coastal and estuarine studies #30. Springer-Verlag, 1988, 471.

3. DRAGERT, H., HORNER, R. 1989, Private communication.

4. DRAGERT, H., ROGERS, G.C., 1988. Could a megathrust earthquake strike southern British Columbia. GEOS, Vol. 17, No. 3, 5-8.

5. DUNBAR, D., LeBLOND, P., MURTY, T.,1989. Maximum tsunami amplitudes and associated currents on the coast of British Columbia. Science of Tsunami Hazards, Vol. 7, No. 1., 3-44.

6. HEATON, T., KANAMORI, H., 1984. Seismic potential associated with subduction in the northwestern United States. Bulletin of the Seismological Society of America, Vol. 74, No. 3, 933-941.

7. HEATON, T., HARTZELL, S.H., 1987. Earthquake hazards on the Cascadia subduction zone. Science, Vol. 236, 162-168.

8. HENRY, R.F., 1982. Automated programming of explicit shallow-water models. Part I, Canadian Technical Report of Hydrography and Ocean Sciences, No. 3.

9. LEMON, D.D., LeBLOND, P.H., OSBORN, T.R., 1979. Seiche excitation in Port San Juan, British Columbia. Journal of Fisheries Research Board of Canada, Vol. 36, No. 10, 1223-1227.

10. LOUCKS, R.H., 1962. Investigation of the 1960 Chilean tsunami on the Pacific coast of Canada. M.Sc. Thesis, University of British Columbia, Vancouver, B.C., 21.

11. MARSHALL MACKLIN MONAGHAN, 1986. Development management in tsunami hazard areas of Port Alberni. Consultants' report prepared for the City of Port Alberni.

12. MURTY, T.S., 1977. Seismic sea waves - Tsunami. Bull. Fish. Research Board of Canada, 198, 337.

13. MURTY, T.S., BOILARD, L., 1964. The tsunami in Alberni Inlet caused by the Alaska earthquake of March, 1964. In W.M. Adams (ed.) Tsunamis in the Pacific Ocean, East West Centre Press, Honolulu, Hawaii, 165-187.

14. MURTY, T.S., EL-SABH, M.I., 1985. Numerical simulation of the tsunami due to a predicted large earthquake in the St. Lawrence estuary. Proceedings International Tsunami Symposium 1985, 75-81.

15. NG, M.K., 1990. Assessement of tsunami hazards on the British Columbia coast due to a local megathrust subduction earthquake, M.Sc. Thesis, University of British Columbia, Vancouver, B.C., 125.

16. ROGERS, G.C., 1988. An assessment of the megathrust earthquake potential of the Cascadia subduction zone. Canadian Journal of Earth Sciences, Vol. 15, No. 6, 844-852.

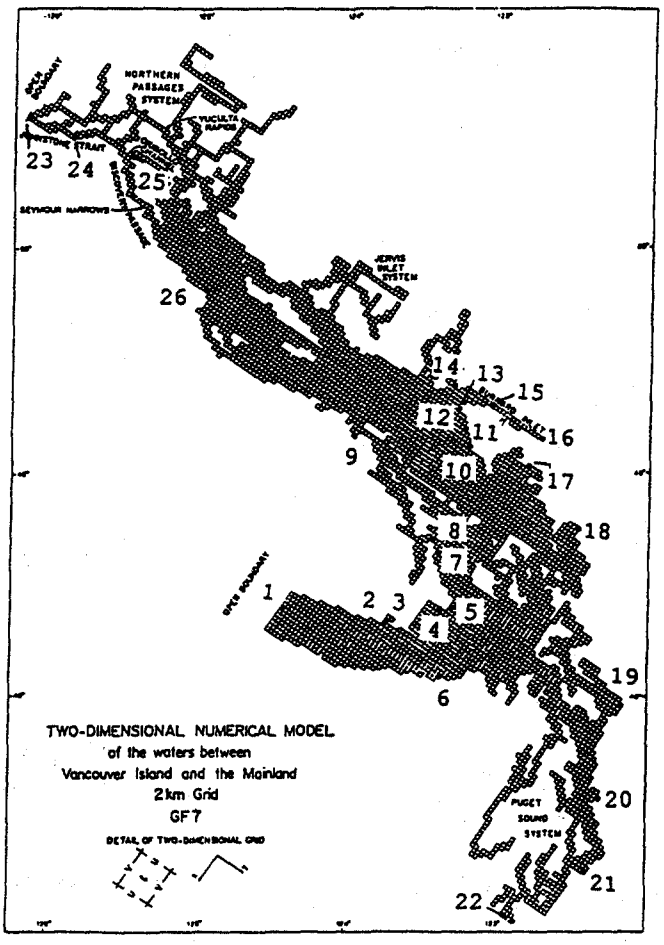

Figure 13: The fine grid layout showing the locations at which time-histories of water level are plotted.

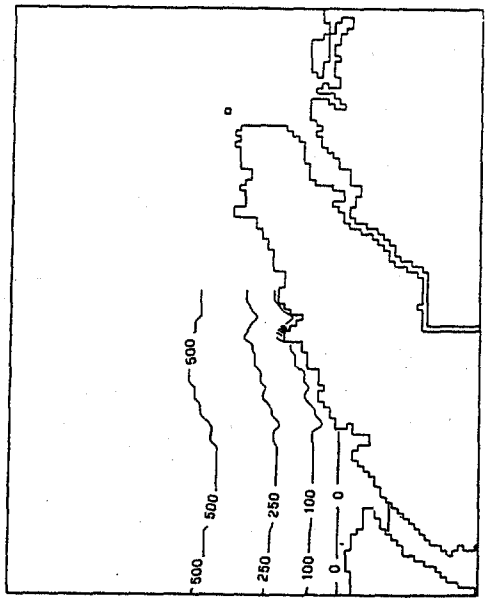

Figure 16: Contours of sea-bottom displacements for the case where the Juan de Fuca segment is ruptured alone. Contour intervals are given in centemetres.

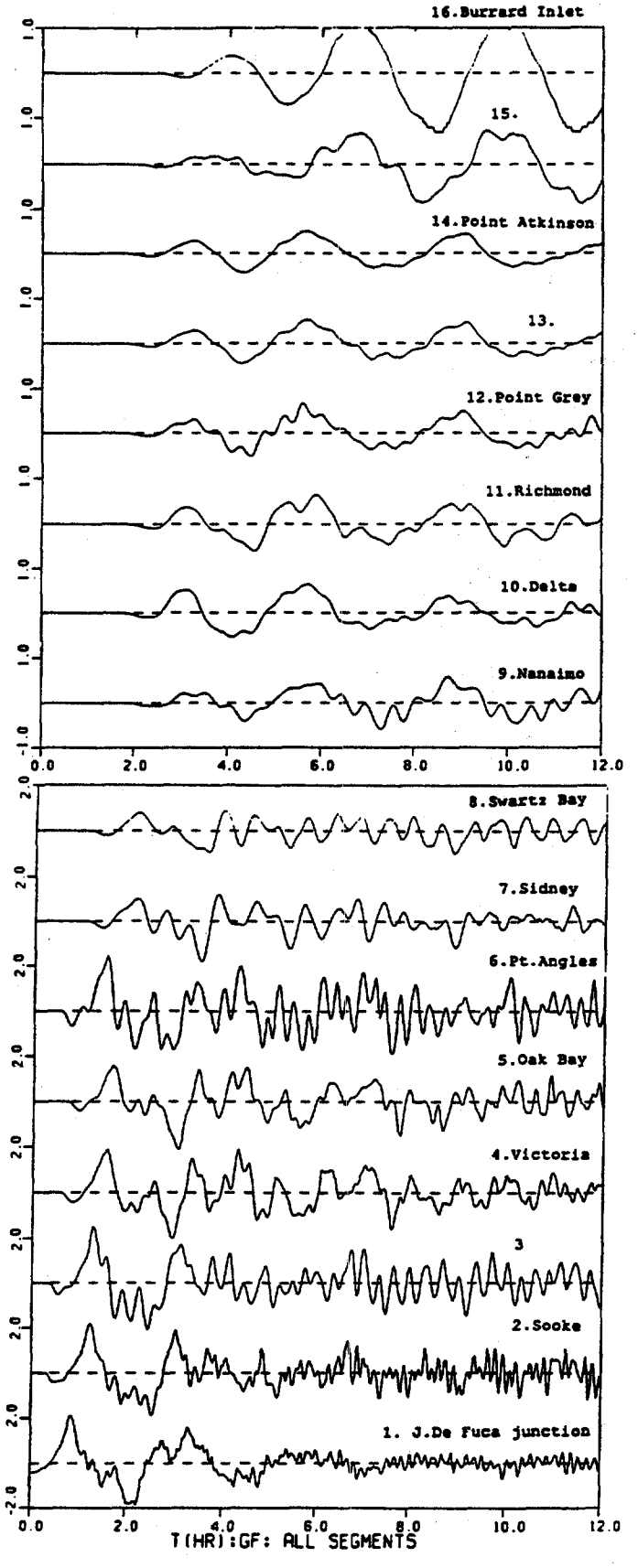

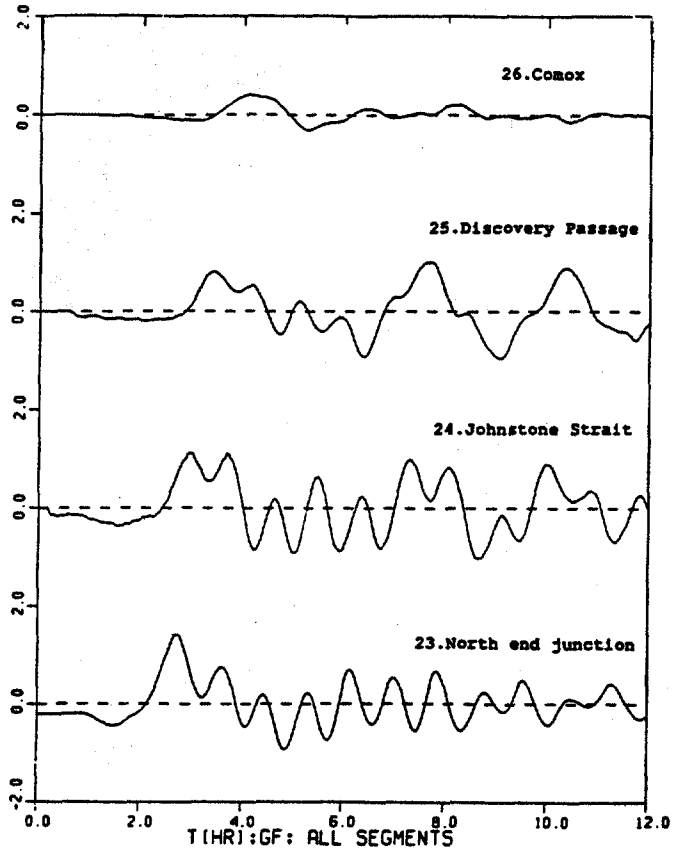

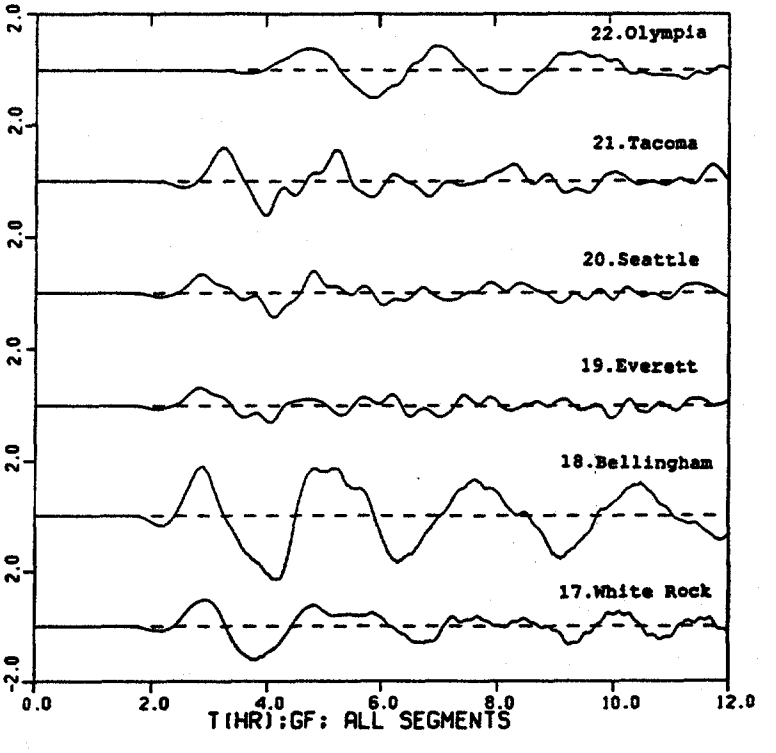

Figure 14: Time-series of computed elevations in the fine grid model for the case of all three segments ruptured together. Station locations are indicated in Fig. 13. The vertical scale is given in metres.

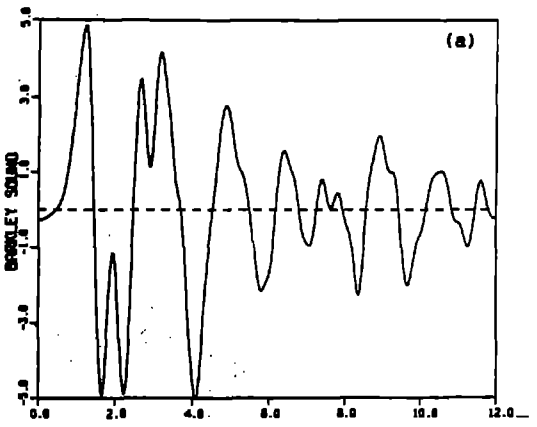

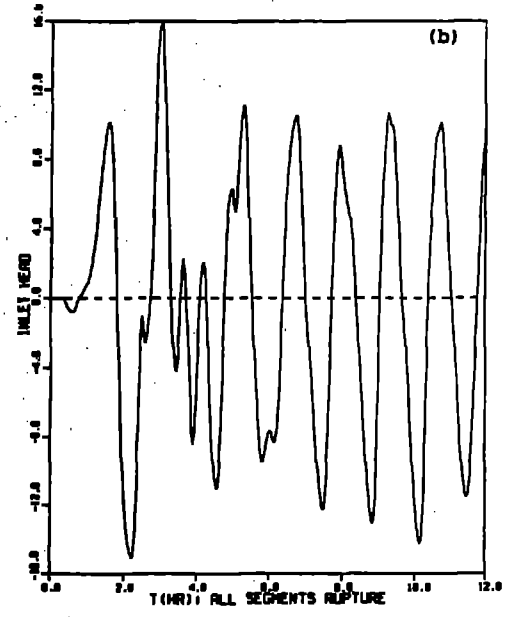

Figure 15: Computed elevations at Alberni Inlet for the case of all three segments ruptured together. The model is driven at Barkley Sound. The vertical scale is given in metres. a) Barkley Sound sea level displacements, b) Inlet head sea level displacements.

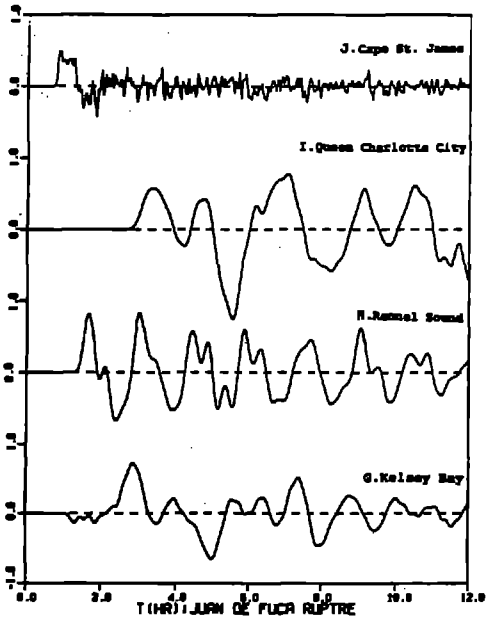

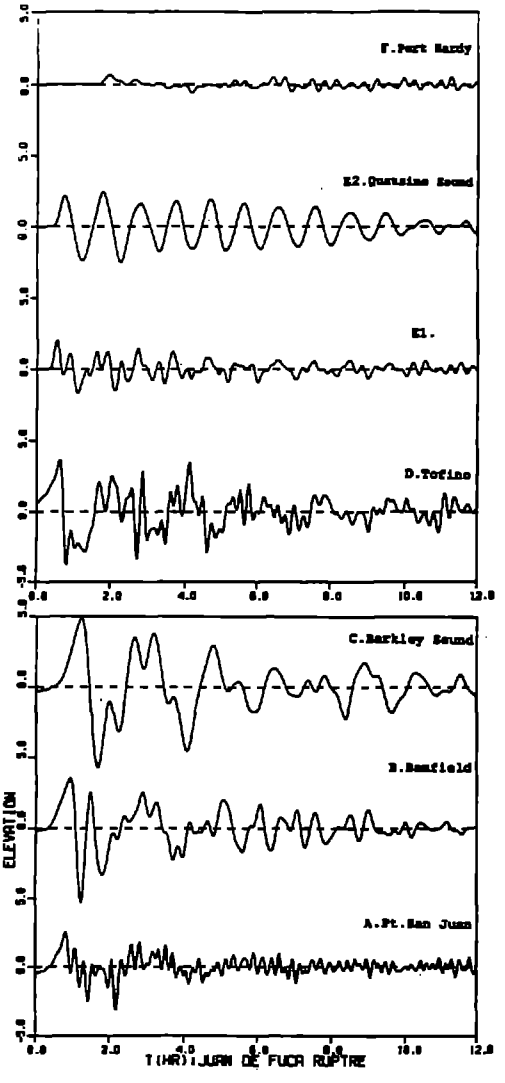

Figure 17: Time-series of computed elevations in the deep-ocean model for the case of the rupture of the Juan de Fuca segment. Station locations are indicated in Fig. 10. The vertical scale is given in metres.

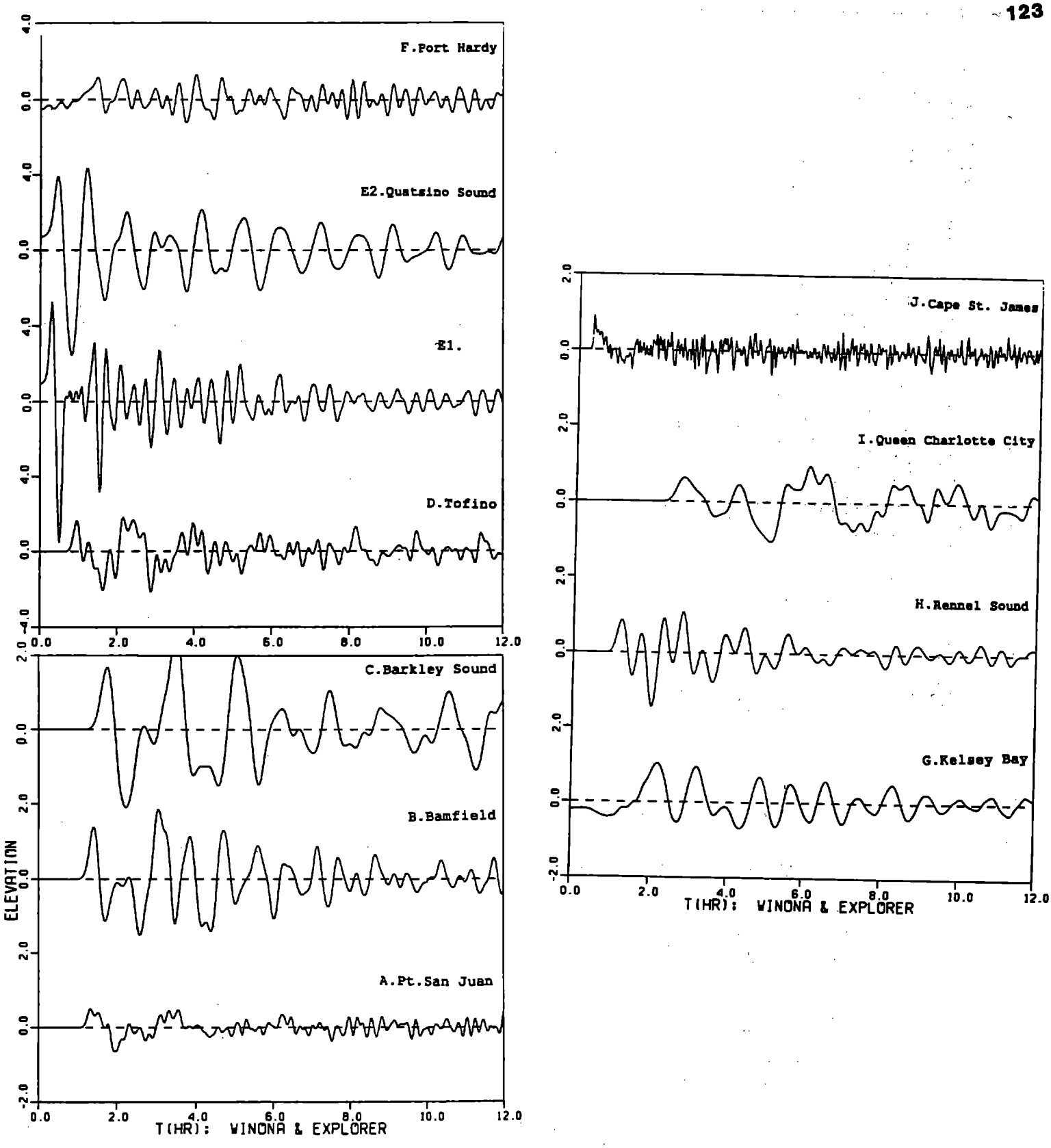

Figure 18: Time-series of computed elevations in the deep-ocean model for the case of the Winona and Explorer segments ruptured together. Station locations are indicated in Fig. 10. The vertical scale is given in metres.

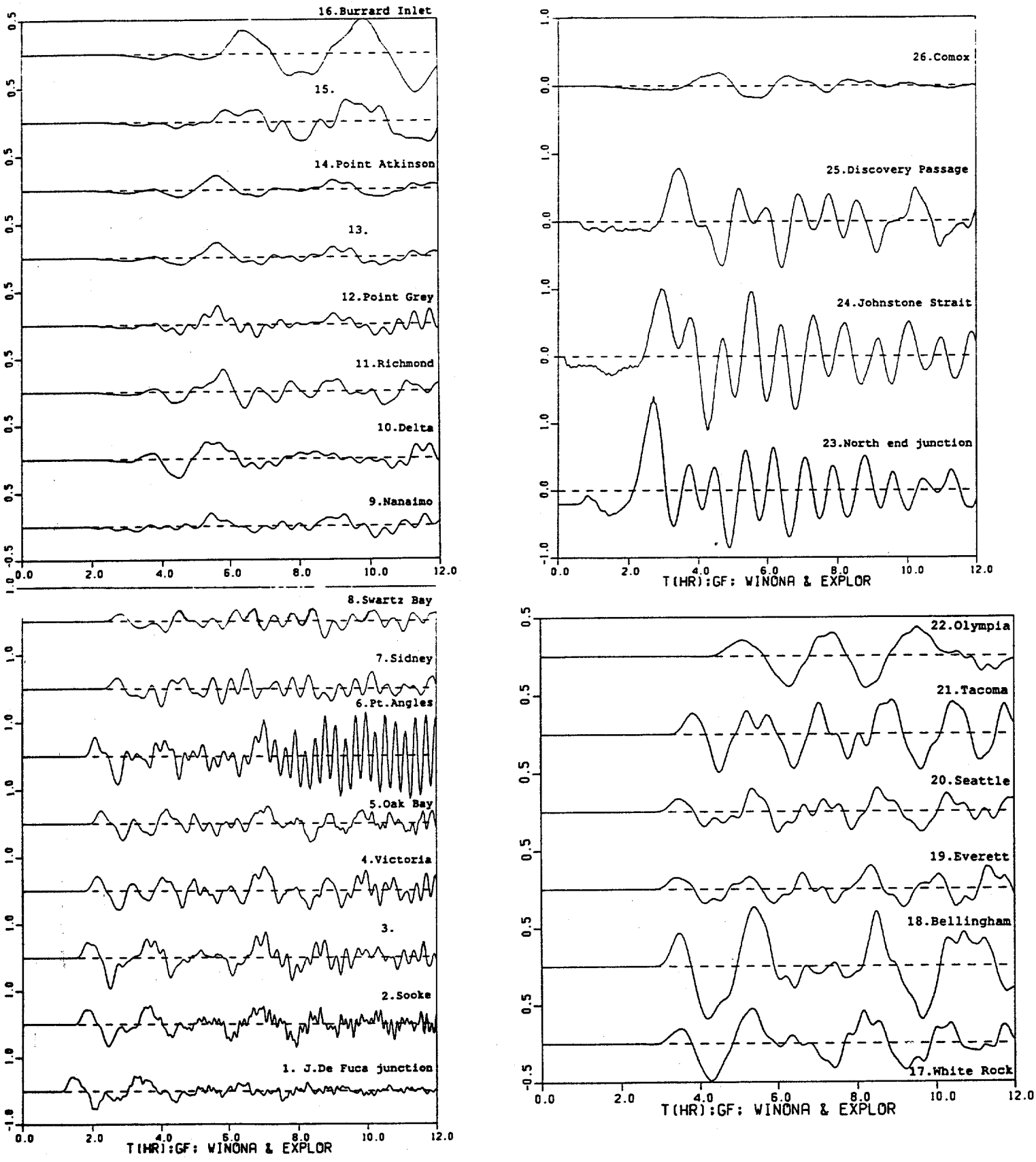

Figure 19: Time-series of computed elevations in the fine grid model for the case of the Winona and Explorer segments ruptured together. Station locations are indicated in Fig. 13. The vertical scale is given in metres.

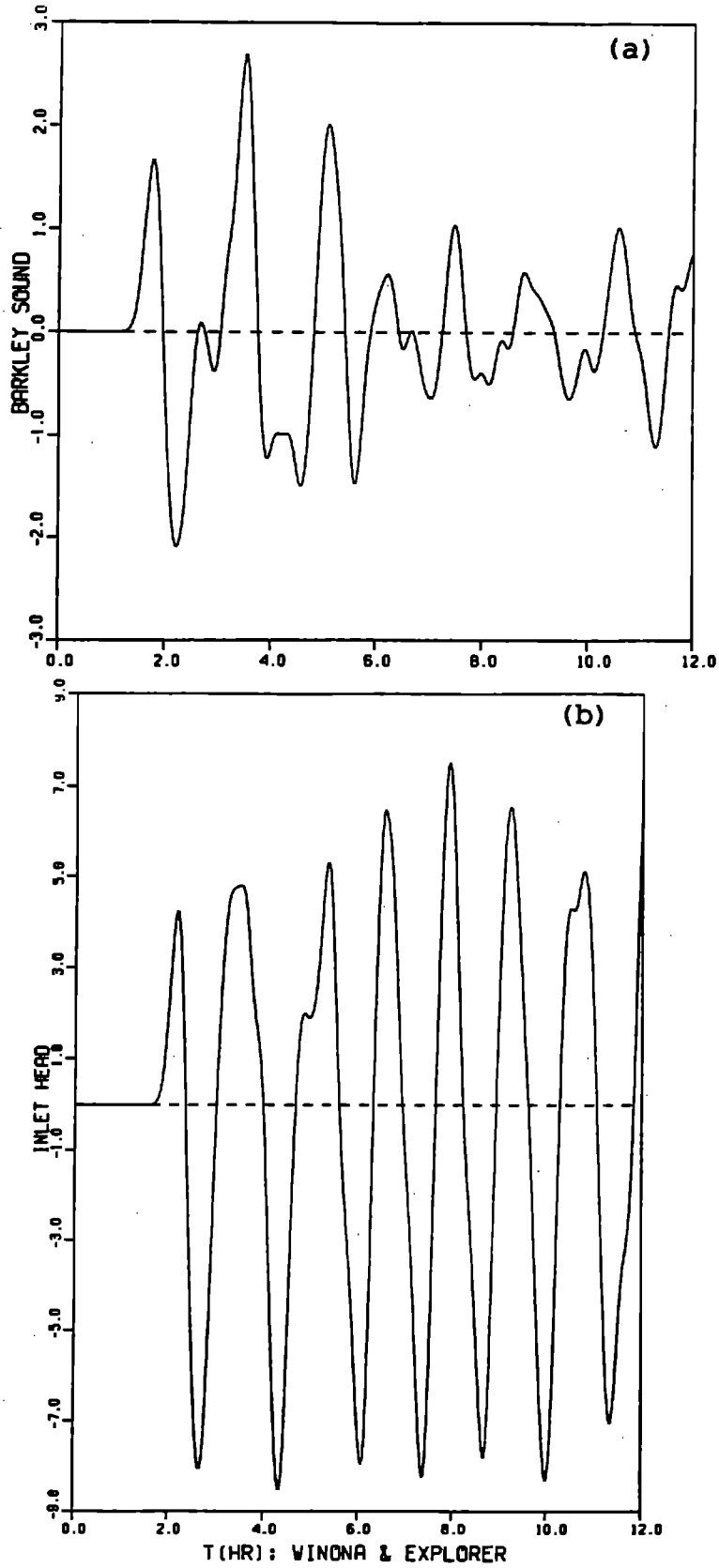

Figure 20: Computed elevations at Alberni Inlet for the case where the Winona and Explorer segments are ruptured together. The model is driven at Barkley Sound. The vertical scale is given in metres. a) Barkley Sound sea level displacements, b) Inlet head sea level displacements.

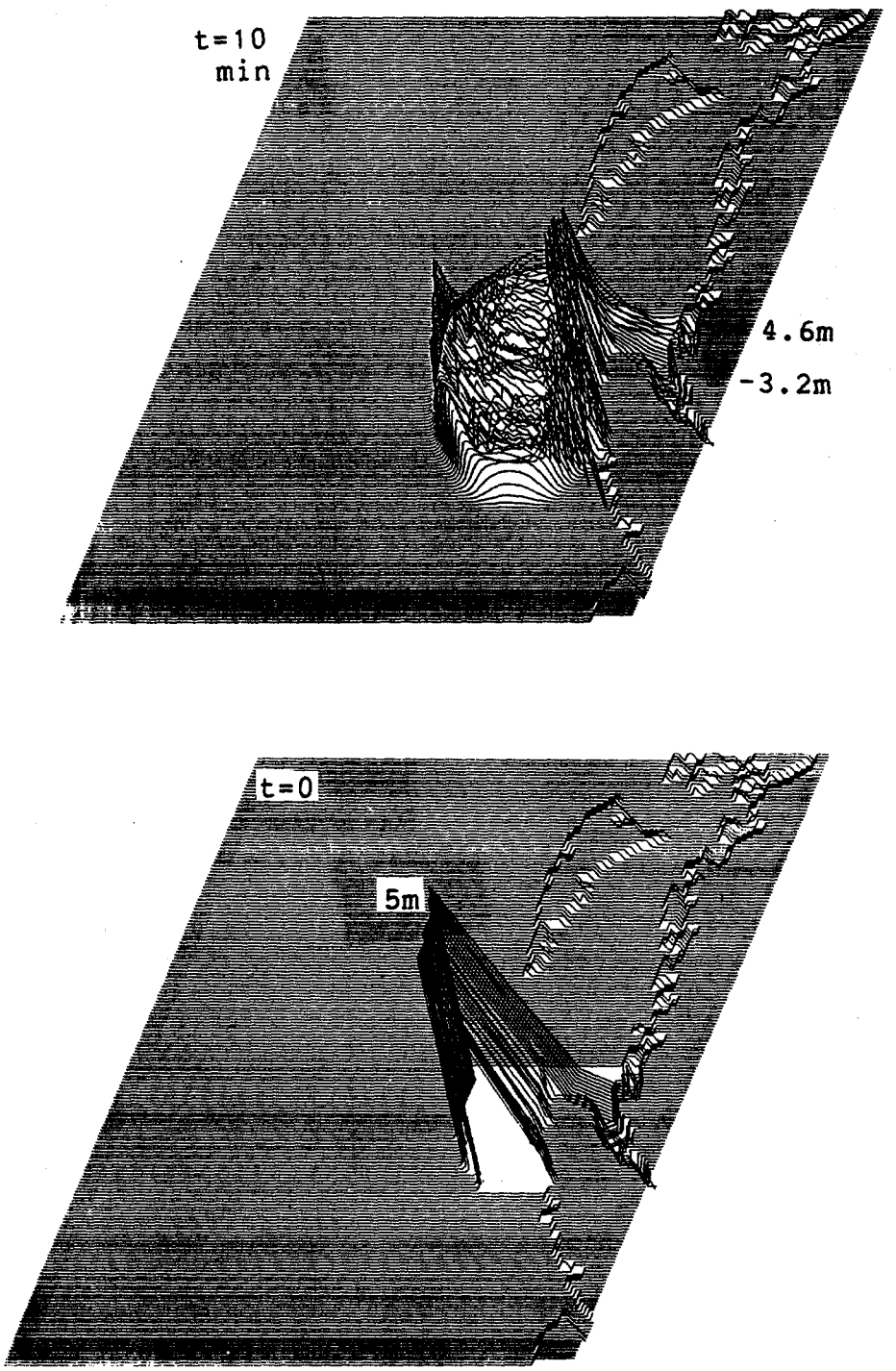

Figure 21: Three-dimensional views of water surface elevations at various time intervals. The shoreline is represented as a 20-cm step. Maximum wave heights are indicated in metres at each plot.

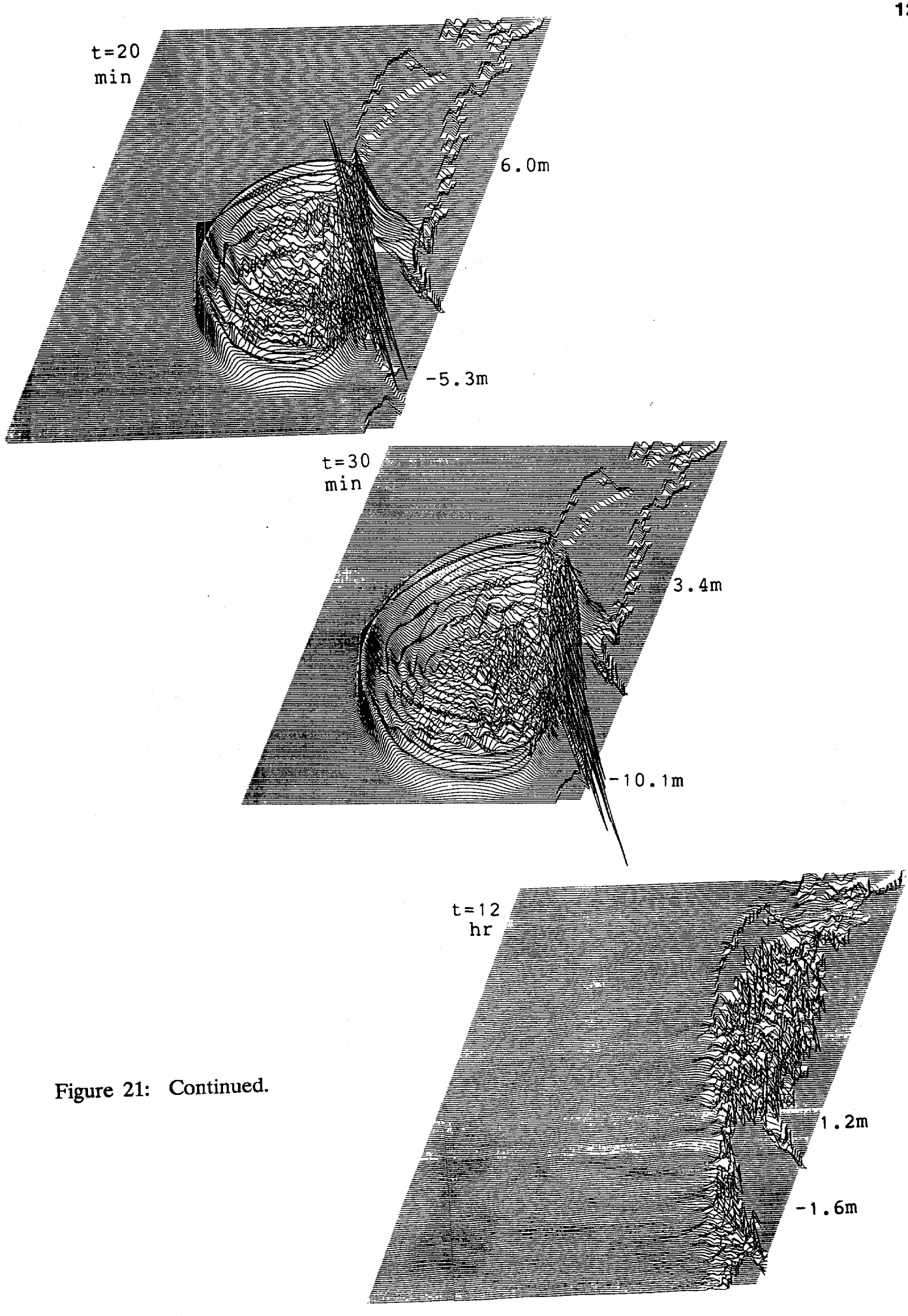

Figure 21: Continued.

APPLICATION FOR MEMBERSHIP

THE TSUNAMI SOCIETY
P.O. Box 8523
Honolulu, Hawaii 96815, USA

I desire admission into the Tsunami Society as: (Check appropriate box.)

☐ Student ☐ Member ☐ Institutional Member

Name _____ Signature _____

Address _____ Phone No. _____

_____

Zip Code _____ Country _____

Employed by _____

Address _____

Title of your position _____

FEE: Student $5.00 Member $25.00 Institution $100.00

Fee includes a subscription to the society journal: SCIENCE OF TSUNAMI HAZARDS.

Send dues for one year with application. Membership shall date from 1 January of the year in which the applicant joins. Membership of an applicant applying on or after October 1 will begin with 1 January of the succeeding calendar year and his first dues payment will be applied to that year.